TWO-DIMENSIONAL INTERPRETATION OF SCHLUMBERGER SOUNDINGS IN SALINE SEDIMENTS

Ketsela Tadesse*
UNU Geothermal Training Programme
National Energy Authority
Grensasvegur 9, 108 Reykjavik
ICELAND

*Permanent address:
Ethiopian Institute of Geological Surveys
Geothermal Exploration Project
P.O.Box. 2302, Addis Ababa
ETHIOPIA

ABSTRACT

The theory of resistivity surveys and resistivity sounding interpretations in geothermal exploration both for one and two dimensions is discussed. Problems in resistivity surveys in general and their possible solutions are discussed. Technical and conditional differences in resistivity surveys in Iceland (National Energy Authority, NEA) and in Ethiopia (Geothermal Exploration Project, GEP) are compared.

Vertical electrical soundings from the Lake Abaya geothermal area in Ethiopia are interpreted in one and two dimensions. Some of these soundings are typical examples of soundings in saline sediments and soundings that are affected by two dimensional geological structures. Saline sediments with a resistivity of 3-5 ohmm and a thickness of about 50 m occupy the Lake Abaya plain. The sediments extend west to the Chewkare fault. These sediments are underlain by an intermidate low resistivity(10-40 Ohmm) substratum. The area west of the Chewkare fault is inferred to have four characteristic layers. These are a high resisistivity layer (greater than 50 ohmm), about 50-200 m thick, which corresponds to the dry and consolidated part of the basalts in the area. Following that comes an intermidate resistivity (10-50 ohmm) layer about 200-400 m thick made of ignimbrite flows, and then a low resistivity layer (less than 5 ohmm) about 400-800 m thick corresponding to a rhyolite sequence, and finally a high resistivity (greater than 50 ohmm) basement that corresponds to precambrian gneisses. Low resistivity around the fault zone on the surface corresponds to the geothermal manifestations, but low resistivity at depth corresponds to the rhyolite zone which may or may not contain geothermal fluid.Along the Chewkau fault this zone is revealed at shallower depth with considerable thickness, and may possibly be the conduit of the hot springs and the fumaroles in the area.

TABLE OF CONTENTS

	Page
ABSTRACT	3
1 INTRODUCTION	
1.1 Scope of work	7
1.2 Introduction to resistivity survey and their interpretation	8
2 THEORY OF RESISTIVITY	
2.1 Introduction	9
2.2 Current flow in homogeneous earth	9
2.3 Measurements of apparent resistivity	12
2.4 The Schlumberger array	13
2.5 Problems with resistivity surveys	13
2.6 Technical and conditional differences between Iceland and Ethiopia	15
3 RESISTIVITY INTERPRETATION	
3.1 The approximate interpretation methods	17
3.2 Iterative interpretation method	18
3.3 Results of one-dimensional resistivity modelling	20
3.4 Resistivity modelling for two-dimensional structures	22
3.5 Discussion	24
3.6 Conclusions	26
4 LAKE ABAYA GEOTHERMAL AREA	
4.1 Geology of the study area	28
4.2 Geothermal manifestations	29
4.3 Geophysical survey	30
4.4 Geothermal model of the Lake Abaya area	33
4.5 Conclusions	33
ACKNOWLEDGEMENTS	34
REFERENCES	35
APPENDIX I	47
APPENDIX II	51

LIST OF FIGURES

Fig. 2.1 General four electrode array 36

Fig. 2.2 The Schlumberger array 36

Fig. 3.1 Ellipse fits to soundings 0.5 W and 1.0 W in line 9 37

Fig. 3.2 Ellipse fits to sounding 0.5E in line 15 and 3.0E in line 9 38

Fig. 3.3 Measured and calculated resistivity pseudo-sections along line 9 38

Fig. 3.4 Two dimensional model and resistivity cross-section along line 9 39

Fig. 4.1 Geological map of Lake Abaya area 40

Fig. 4.2 Measured and calculated resistivity pseudo-section along line 15 41

Fig. 4.3 Two dimensional model and resistivity cross-section of line 15 42

Fig. 4.4 Measured and Calculated resistivity pseudo-section along line 17 43

Fig. 4.5 Two dimensional model and resistivity cross-section of line 17 44

Fig. 4.6 Measured and calculated resistivity pseudo-sections along line 14 45

Fig. 4.7 Two dimensional model and resistivity cross-section along line 14 46

1 INTRODUCTION

1.1 Scope of work

This report is a part of the work undertaken by the author during six months training at the United Nations University Geothermal Training Programme held from April to October 1984 in Iceland at the National Energy Authority (ORKUSTOFNUN) under the sponsorship of the United Nations University and the Government of Iceland.

The training started by a four weeks introductory lectures course covering the main aspects of geothermal exploration and the sciences of geothermics.The following topics were discussed by different lecturers; present status of geothermal development, planning of geothermal projects, geological, geochemical, geophysical, and hydrological methods of exploration, borehole geology, borehole geophysics, different aspects of engineering, geothermal resource assesment and geothermal utilization.

The author participated in specialised training for one week in head-on profiling measurements at Krafla (Northern Iceland), two days in Schlumberger sounding measurments in the Trolladyngja area(in S-W Iceland) and one week in geological mapping of structural features that control the flow of geothermal fluids around Egilsstadir and Akureyri. The author also participated in a two weeks field excursion to the main high and low temperature geothermal areas of Iceland, and visited several factories that benefit from geothermal energy.

Finally, the last ten weeks of the training were used for one and two dimensional interpretation of Schlumberger resistivity soundings using computer programs. Soundings that are affected by saline sediments and two dimensional structures such as faults and dykes were the main concerns of the author. The exercise was carried out using soundings from the Lake Abaya geothermal area that were collected by the author himself and his colleagues in Ethiopia.

1.2 Introduction to resistivity surveys and their interpretation

Various electrical methods have been used extensively in geothermal exploration. Resistivity methods are of particular importance in mapping fault zones, fracture zones and contacts of different geological units. Thermal waters become less resistive with increasing salinity and with increasing temperatureup to 300°C. The effect of temperature < 300°C is to enhance conductivity of the water in the pores of the rock by decreasing the viscosity, however, above this particular temperature the resistivity increases.

It is not only temperature and salinity that affect the resistivity of rocks. An increase in the water content (porosity) and in the assemblage of conductive minerals (products of alteration) can also decrease the resitivity significantly. These are phenomena that we encounter most of the time in geothermal activity.

There are several techniques to study subsurface electrical structures, namely the Schlumberger sounding method, dipole-dipole traversing method, the magneto telluric method and the elctromagnetic method. The objective of all these methods is to map electrical structures at depths which are meaningfull in terms of geothermal exploration.

The use of electrical method, is becoming increasingly useful through advances in both equipment and interpretations in recent years. Until recently, the interpretation of electrical resistivity data has been done with the assumption of horizontal layer stratification. This was because master curves and one dimensional computer interpretation methods were based on the principle of horizontal stratified models. Recent techniques allow a much more sophisticated interpretation of the geological structures. More realistic model of the subsurface can be constructed by looking for the variations of resistivity in two directions. Through analog and numerical modelling techniques for two dimensional geological structures, great advances have been made, (Mufti 1976, Dey and Morrison 1976).

2 THEORY OF RESISTIVITY

2.1 Introduction

Among the electrical methods, resistivity prospecting is superior to all the others. The purpose of resistivity surveys is to investigate changes in the resistivity of formations with depth as well as laterally. An artificial source of current is driven into the ground through electrodes. The potential difference is measured between two electrodes in the area of the current flow, named potential electrodes. Whenever there is a change in resistivity of formations there is also a change in the form of the current flow introduced into the ground and this distortion of current also affects the value of the potential difference. This canoften be accomplished by changing the distance between current electrodes where the center of the configuration and its orientation remain fixed. In inhomogeneous earth the presence of three dimensional bodies such as dykes, faults, vertical and horizontal contacts between geological units affect the potential at the surface. In fact this effect depends on the location, shape, size and on the electrical resistivity of the structures themselves. Therefore it is possible to detect the presence of anomalous resistivity of these various structures by measuring the potential at the surface.

2.2 Current flow in homogeneous earth

To approach the study of earthwith resistivity measurements, let us first consider the case of a completely homogeneous isotropic earth. The flow of current in a medium is according to the principle of conservation of charge.

$$\mathrm{div}\vec{j} = \frac{\partial q}{\partial t} \qquad \text{eq. 2.1}$$

where q = the charge density (c/m3); j = the current density (A/m2); For stationary current $\partial q/\partial t$ will be zero and the above relation becomes

$$\text{div}\vec{j} = 0 \qquad \text{eq. 2.2}$$

According to Ohms law if ρ is the resistivity of the medium the current density j is related to the electric field intensity E (V/m) as follows.

$$\vec{j} = \frac{1}{\rho}\vec{E} = -\frac{1}{\rho}\,\text{grad}V \qquad \text{eq. 2.3}$$

Where V is the electric potential in volts.

For an isotropic medium j is the same in all directions and has the same direction as E. In an anisotropic medium, however, j has a directive property and is not in the direction of E. From eq. 2.2 and eq. 2.3 for isotropic medium we get

$$\nabla\cdot(\frac{1}{\rho}\,\vec{\nabla}V) = 0 \qquad \text{eq. 2.4}$$

This can be treated further as

$$\vec{\nabla}(\frac{1}{\rho})\cdot\vec{\nabla}V + \frac{1}{\rho}\cdot\vec{\nabla}\cdot\vec{\nabla}V = 0 \qquad \text{eq. 2.5}$$

This is the basic equation of electrical prospecting using direct current. Since the medium is assumed to be homogeneous ρ is independent of the coordinate axes and eq. 2.5 reduces to

$$\vec{\nabla}\cdot\vec{\nabla}V = 0 \quad \text{or} \quad \nabla^2V = 0 \qquad \text{eq. 2.6}$$

Therefore the electrical potential distribution for direct current flow in homogeneous isotropic medium satisfies Laplaces equation.

Now let us assume that a current I is introduced into an infinite homogeneous medium at a certain point p. Then the potential at a distance r from p will only be a function of r, therefore Laplaces equation can be written as

$$\frac{d^2V}{dr^2} + \frac{2}{r}\frac{dv}{dr} = 0 \qquad \text{eq. 2.7}$$

which has the solution

$$V = C_1 + \frac{C2}{r} \qquad \text{eq. 2.8}$$

When the potential is taken to be zero at infinite distance from the source the integration constant $C_1 = 0$.

It is known that the equipotential surfaces are spherical and the electric field lines as well as the current lines are radial. The current density at a distance r may be written as

$$\vec{j} = -\frac{1}{\rho}\cdot\frac{\partial V}{\partial r} = \frac{1}{\rho}\cdot\frac{C_2}{r^2} \qquad \text{eq. 2.9}$$

Then the total current passing through the spherical surface of radius r is

$$4\pi\cdot r^2\cdot j = \frac{1}{\rho}\cdot 4\pi\cdot C_2 \qquad \text{eq. 2.10}$$

For a semi-infinite medium, when the current is introduced into a homogeneous ground, the total current flowing out of a hemispherical surface of radius r is given by the relation

$$2\pi\cdot r^2\cdot j = \frac{1}{\rho}\cdot 4\pi\cdot C_2 \qquad \text{eq. 2.11}$$

and the constant is equal to $I\rho/2\pi$.

Thus in a homogeneous medium, the potential V due to a point source is inversely proportional to the distance r. It is also directly proportional to the current I emanating from the source and to the resistivity ρ of the medium i.e

$$V = \frac{I\rho}{2\pi}\cdot\frac{1}{r} \qquad \text{eq. 2.12}$$

Practically, the current is injected into the ground by means of two electrodes, where one is a source and the other a sink, and the potential at any point due to these two points is

$$V = \frac{I\rho}{2\pi}\cdot\left(\frac{1}{r_1} - \frac{1}{r_2}\right) \qquad \text{eq. 2.13}$$

Where r_1 and r_2 are the distance of the point p from the source and the sink respectively.

2.3 Measurements of apparent resistivity

Equations 2.12 and 2.13 can be solved for ρ, in terms of the potential difference ΔV, the current I and the distance between the electrodes. The value obtained for ρ by substituting a measured value of ΔV and I in a realistic case where the subsurface is non homogeneous is called apparent resistivity.

Consider a direct current of strength I driven into a homogeneous and isotropic earth through point electrode A(source) and B(sink). (Fig. 2.1).

The potential difference between the two points M and N on the surface is given by

$$\Delta V = \frac{I\rho_a}{2\pi}\left(\left(\frac{1}{AM} - \frac{1}{BM}\right) - \left(\frac{1}{AN} - \frac{1}{BN}\right)\right) \qquad \text{eq. 2.14}$$

which can be written as $\Delta V = \frac{I\rho_a}{2\pi}\cdot G$

solving for ρ we get the following relation

$$\rho_a = \frac{2\pi}{G}\cdot\frac{\Delta V}{I}$$

where 1/G is the geometric factor.

2.4 The Schlumberger array

The Schlumberger array shown in Fig. 2.2 is the most widely used array in resistivity surveys to determine the apparent resistivity. It is designed to measure the potential difference between twoadjacent points. These two points are held stationary for several lengths of AB. The value obtained by successively increased distance of AB is the apparent resistivity and the values are plotted on a log-log paper against AB/2. This is called vertical electrical sounding.

Using equation 2.14 we can derive the relation for the potential difference and then the apparent resistivity from Fig. 2.2.

$$\Delta V = \frac{I\rho_a}{2\pi}\left(\left(\frac{1}{C-P}-\frac{1}{C+P}\right)-\left(\frac{1}{C+P}-\frac{1}{C-P}\right)\right) \qquad \text{eq. 2.15}$$

This reduces to

$$\Delta V = \frac{2I\rho_a}{\pi}\cdot\frac{P}{C^2-P^2} \qquad \text{eq. 2.16}$$

the expression for ρ_a is then

$$\rho_a = \frac{\pi}{2}\cdot\left(\frac{C^2-P^2}{P}\right)\cdot\frac{\Delta V}{I} = \frac{\pi}{2}\cdot K\frac{\Delta V}{I} \qquad \text{eq. 2.17}$$

where $K = (C^2-P^2)/P$ is the geometric factor depending on the distance between the electrodes.

2.5 Problems with resistivity surveys

As in most other geophysical methods, some problems can arise in resistivity surveys which can be solved only partly. To begin with, most geothermal areas are characterized by tectonically disturbed and irregular sub-surface inhomogeneities. Then due to near surface inhomogeneities it is possible to encounter distorted potential field at the measuring potential electrodes and misleading results can be obtained if the center of the sounding is sited over

shallow hetrogeneities. Measurement points should therefore not be sited in areas where the potential electrodes encouter inhomogeneous surfaces.

Effect of topography is one of the problems in geothermal areas. Ward and Sill (1983) have pointed out that topographic effects are important where slope angles are greater than 10 degrees for slope lengths of one dipole or more. The solution of the problem is to include the topographic surface in numerical models used for interpretation.

The existence of a conductive overburden, such as marshy, porous alluvium, highly weatherd rocks, which are areas of high current density concentration, hinders current from penetrating to the more resistive medium. In such areas the detection of the bed rock is certainly more limited than when there is no overburden. The solution of this problem is to interpret soundings of such areas by the two dimensional method. This approach can give the lateral and vertical extent of the conductive layer including the physical parameters.

Man made appliances such as wirefence or ironpiles, metallic pole power lines plugged in the ground, borehole casings and pipelines affect the current flow from the desired position and redistribute the current flow from the grounded wire source through themselves. These materials also create a path for various interfering signals, however, this can be avoided by putting the measurement points far from these materials.

Natural field noises such as thunderstorms, telluric currents or natural electric and magnetic fields which are dependent on the interaction of particles and fields emanated from the sun with the earths magnetic field affect resistivity measurements.

2.6 Technical and conditional differences between Iceland and Ethiopia

During the field training the author and his friends participated in VES (vertical electrical sounding) data collection using Schlumberger array inthe Trolladyngja area and head-on profiling measurements in Krafla (Iceland). The main differences observed between field practices in Ethiopia and Iceland are as follows.

a) In the GEP in Ethiopia we use mostly the relations between MN and AB as 1/7AB less or equal to MN less or equal to 1/5AB and maximum AB/2 length of 3160 m. In the geopysical surveys of NEA, small MN/2 down to 0.5 m are used and the usual maximum AB/2 used is 1780 m. In the first decades the GEP's surveys readings are scares and few AB/2s are used but in the NEA's surveys several readings and several overlaps are available. The importance of several readings and several MN/2 is that the curve will have a regular appearance without loosing all the information at the top, and the curve will be interpretable. The cable lay out is also important. The one used by NEA is more progressive and the facilities are better. For example, to measure the potential difference at different MN/2 positions, numereous cables of different lengths lumped together are connected to a selector.

b) The transmitters in both GEP and NEA use current with relatively long period or low frequency to minimize the effect of polarization. But the one used by NEA has the advantage of being connected with the receiver to simulate it to start recording the potential difference.

c) The receivers record many readings and give the mean potential difference both in GEP and NEA. The receiver used by NEA has got the advantage of displaying each single reading, number of readings and the standard deviation which enables the operator to follow what is happening and the quality of the data. In the case of the GEP it is possible to follow and see what is happening just by looking at the pointer which is made for this purpose on

the receiver. Recently a new receiver has been made at NEA, it has three receivers all of them mounted in the same box and measures three different MN/2 at the same time.

d) The power source used by NEA consists of two 12 Volts/75 Amphr batteries coupled together in series, but a.c generators are in use at GEP. The power source used by NEA weighs 15 - 20 kg, but in GEP 50 - 100 kg and sometimes a generator which is mounted on a trailor or pickup Land Rovers.

e) For measuring AB/2 and MN/2 lengths the wires are marked at different measured intervals to facilitate direct measurements of AB/2 and MN/2 lengths in field surveys at NEA, whereas costly theodolite surveys are applied in GEP. This is partly due to the rough topography and the vegetation cover in the surveys areas.

f) GEP uses thicker wire and thicker insulation for the purpose of leakage prevention and greater durability in its hardness. Because of this the reels are much heavier in GEP than in NEA.

g) Grounding: In most geothermal areas in Ethiopia the contact resistance is high because of the dry soil on the surface. In order to lower the contact resistance we use aluminium or cupper sheets, wire mesh, salt and water in addition to electrodes.

h) Because of the heavier equipment items (c,d,e) GEP uses more manpower than NEA.

i) The computer facilities are very different, NEA has got the VAX/VMS 750 computer by which many sophisticated programmes can be used and facilitates easy work. GEP has a Hewlett Packard mini-computer which can be handled only by a single user at a time. More over it has a limited computer space. Hopefully, GEP will soon obtain access to a large computer.

3 INTERPRETATION OF RESISTIVITY SOUNDINGS

The mathematical analysis of quantitative interpretation of resistivity surveys is developing from day to day. Fruitful results have been obtained recently in consideration of resistivity varations in two directions and three dimensional view of resistivity variation and its interpretation is shaping its way towards sophistication. The assesment of highly qualified interpretation should progress from rough preliminary assumptions and estimates made in the field. Thus beginning with the simplest and building up to the complex keeps the work up-to-date and effective to perform as well as to obtain tangible results.

3.1 The approximate interpretation methods

The auxiliary point method has been extensively used for the interpretation of resistivity soundings. The first step to consider in this method is the selection of short segments of an apparent resistivity curve and to identify to which group of curve it belongs, i.e wether it belongs to a bell (K)-type,a bowl (H)-type,an ascending (A)-type or a descending (Q)-type for interpretation using the standard curves. In doing so one has to bear in mind that a branch of an apparent resistivity curve is a segment that expresses the transition from one layer or subsurface to another. The point on the graph of two or a three layer apparent resistivity curve, usually marked by a cross has as coordinatesthe thickness and the resistivity (ordinate) of the top layer.

The auxiliary point method uses the approximation of each segment of an apparent resistivity curve by a two layer curve. The ordinates of the cross of this two layer curve are concidered to represent the thickness and the resistivity of a fictitious layer that replaces the sequence of shallower layers. The fictitous layer is then used to analyse the proceeding portion of the curve. Detailed procedure of the method is beyond the scope of this report, but the author would like to recommend Koefoed (1979) for further clarification. Following the auxiliary point method that makes uses of two layer

apparent resistivity model curve is three layered curve. Specific examples and interpretation procedures are best described by Koefoed (1979) and Keller and Frischnet (1966).

The advantages of the approximate interpretation methods are: It helps to obtain an approximate picture of the survey area and leads to conclusions where to concentrate future planning of the work. It helps as a primary working model for the improved delineation of the target area, and it helps as a starting point for the exact interpretation and allows speedy applications.

3.2 Iterative interpretation method

Iterative interpretation methods are presently found to be the best methods of interpreting resistivity soundings. These methods make use of comparisons of the field data with theoretical values based on the data obtained by the approximate interpretation method. If the agreement between the two fails, the parameters of the layers obtained by an approximate method are changed in such a way that it is suitable to fit the field data. The procedure will be repeated until a suitable agreement is found. Various authors have published varieties of iterative interpretation methods, in which the computation of the parameters can be adjusted by the computer itself. The computer program used for the one dimensional interpretation of Schlumberger soundings in this report is the ELLIPSE method. The program was written and developed by the staff of NEA. This program makes use of the expression for the potential at the surface of a layered earth given by the relation

$$V = \frac{\rho 1 I}{2\pi} \int_0^\infty K(\lambda) \cdot J_o \cdot (\lambda r) d\lambda \qquad \text{eq. 3.1}$$

where $K(\lambda)$ = Kernels function; $J(\lambda r)$ = Bessels function of order 0.

Considering the expression for ρ_a in a symmetrical electrode configuration with the current electrodes on the outside where C is the current electrode distance; P is the potential electrode distance then the potential difference ΔV means

$$\Delta V = 2\,(V(C-P) - V(C+P)) \qquad \text{eq. 3.2}$$

This yields

$$\rho_a = 2\rho_1 C\left(\frac{C^2 - P^2}{4PC}\right)\int_o^{\infty} K(\lambda)\left[J_o(\lambda C-\lambda P) - J_o(\lambda C+\lambda P)\right]d\lambda \qquad \text{eq. 3.3}$$

Thus the program ELLIPSE is made to calculate this equation as a function of both the potential and the current electrode distances. i.e

$$\rho_a(C,P) = 2\rho_1 C\cdot\frac{C^2 - P^2}{4CP}\int_o^{+\infty} K(\lambda)\left(J_o(\lambda C-\lambda P)-J_o(\lambda C+\lambda P)\right)d\lambda \qquad \text{eq. 3.4}$$

If $P << C$ then

$$\rho_a = -\frac{2\pi C^2}{I}\left(\frac{\partial V}{\partial r}\right)\Big|_{oP5} \qquad \text{eq. 3.5}$$

Where ρ_a is the Schlumberger apparent resistivity. Now we know that for every fixed potential electrode distance

$$\rho_a\,(C,P) \rightarrow\rightarrow\rightarrow \rho_a\,(C) \qquad \text{eq. 3.6}$$

as C goes larger and larger. If we define the following as $P_1 < P_2 < \ldots < P_n$ are different MN/2 values in the measurement $f_1, f_2, f_3, \ldots\ldots f_{n-1}$ are correction factors so that

$f_{n-1}\cdot\rho_a\,(C,P_{n-1})$ coincides with $\rho_a\,(C,P_n)$ at infinity.
$f_{n-2}\cdot\rho_a\,(C,P_{n-2})$ coincides with $\rho_a\,(C,P_{n-1})$ at infinity.
$f_{n-3}\cdot\rho_a\,(C,P_{n-3})$ coincides with $\rho_a\,(C,P_{n-2})$ at infinity.
- - - - - -
- - - - - -
- - - - - -
$f_2\cdot\rho_a\,(C,P_2)$ coincides with $\rho_a\,(C,P_1)$ at infinity.

Now if we calculate for P_1

$f_1 \cdot f_2 \cdot f_3 \cdot \ldots . f_{n-1} \cdot \rho_a$ coincides with ρ_a (C, P_{n-1}) at infinity. Then the parameters that are necessary to calculate the curve are

$\rho_1, \rho_2, \rho_3, \ldots\ldots \rho_n$ - the resistvities
$t_1, t_2, t_3, \ldots\ldots t_n$ - the thickness
$f_1, f_2, f_3, \ldots\ldots f_{n-1}$ the corection factors.

These parameters are then formulated applying the non-linear least squares method. By taking the logarithms of the squares the inversion is found. Based on this principle the program calculates a theoretical curve that fits the field curve for each overlap. The quality of the fit between the field curve and the calculated curve is defined by a statistical criteria so that the percentage error of the fit can be recognised. If the error is high and improvement of the quality of the fit of the curve is desired, easy applicable method of changing parameters i.e the resistivity and thickness is used. In such a way the program itself selects reasonable parameters that fits to the field curve once it is given a starting model. However, the initial model should be reasonable so that, the error will be minimized and good results can be obtained in a short time. If a starting model is not at least a rough approximation of the reality, the interpretation tends to converge slowly or even fails to converge. The apparent resistivity curve is used for comparative purposes. Computed curves are always compared with the measured apparent resistivity curve.

3.3 Results of one-dimensional resistivity modelling

Since geothermal areas are characterised by complex geological structures it is impossible to find uniform horizontally layered earth. Structures like faults and dykes which result in dipping or vertical contacts create non-horizontal uniform layered earth. Soundings made over non-horizontal layers are characterised by sharp rises exceeding the maximum 45 degrees slope. In order to fit these branches of steeply rising curves the one dimensional

interpretation increases the resistivity value of the basement layer to an unbelivable extent. To explain this let us consider the following soundings in Fig 3.1 and Fig 3.2which fromthe northwestern sector of the Lake Abaya geothermal area in Ethiopia. Figure 3.1 shows soundings 0.5W and1.0W along line 9 in an east-west orientation. If we take the slope between AB/2 = 2000 and AB/2 = 3200 m in both cases we get more than 60 degrees. Using the computer program ELLIPSE mentioned in section 3.2, the data is treated to find possible parameters of each layer. As can be observed in the Figure, the fits at the end segments of the curves are poor. Models of 5 and 6 layers are used to find the appropriate fit. If we concentrate on one of them, i.e taking 0.5W it has 5 layers one dimensionally. However, the fit beyond AB/2 = 2400 m is very poor. It is possible to say that this sounding has got a two dimensional effect due to vertical contacts, because the sounding is sited on a horst like structure where both sides of the measurement could encounter vertical displacements (normal faults) by which the effect could be explained clearly.

Soundings of saline sedimentary areas are characterised by more gentle or even constant progression in the first and second decade with relatively low values. But their final segment does usually exceed 45 degrees and is difficult to fit. Even if a fit is found, the resistivity contrast will be high and non-relevant. Fig 3.2 shows typical soundings over a sedimentary area taken from Lake Abaya. Soundings 0.5E on line 15 and 3.0E on line 9 from left to right respectively are taken as examples out of the soundings that are made within the lakustrine sediments of the Abaya plain. Selecting 0.5E of line 15, the upper part of the curve has low resistivity values which are mainly due to the high conductivity of the salt solution within the sediment. But as it encounters the substratum it rises steeply. This sounding was interpreted by making 3 layered model one dimensionally. In the first part, the theoretical calculation and the field data agree with each other but there arises the impossibility for the final segments. So this is truly a two dimensional effect. In general most of the soundings in the lakustrine sediments have the same appearance and the one dimensional interpretation is

unsatisfactory therefore a two dimensional approach to the problem is necessary. In addition to this the thickness of the sediment and the substratum could be determined.

3.4 Resistivity modelling for two-dimensional structures

Dey and Morrisson (1976) have proposed a direct and explicit finite difference technique in order to solve for the potential distribution due to a point source. The apparent resistivity values at few electrode positions are computed using the algorithm of the finite difference method discussed by Dey and Morrisson (1976).

The flow of current over a volume based up on the principle of conservation of charges will have the following relations

$$\vec{\nabla}\cdot\vec{J} = \frac{\partial q}{\partial t}\,\delta(x)\delta(y)\delta(z) \qquad \text{eq. 3.7}$$

where J is the current density; q is the charge of density at a point in the cartesian space

If Φ is the potential at a point (x,y,z) and $\rho(x,y,z)$ is the resistivity of the medium at a point (x_s,y_s,z_s) then by Ohms law,

$$\vec{J} = -\frac{1}{\rho(x,y,z)}\,\vec{\nabla}\Phi(x,y,z) \qquad \text{eq. 3.8}$$

But we can relate the resistivity and the conductivity as

$$\frac{1}{\rho(x,y,z)} = \sigma(x,y,z)$$

Where $\sigma(x,y,z)$ is the conductivity of the medium. Using this relation then eq.3.7 will take the following form

$$-\vec{\nabla}\cdot\left[\sigma(x,y,z)\vec{\nabla}\Phi(x,y,z)\right] = \frac{\partial q}{\partial t}\delta(x_s)\cdot\delta(y_s)\cdot\delta(z_s) \qquad \text{eq. 3.9}$$

applying vector calculus equation (3.9) becomes eq. 3.10

$$\vec{\nabla}\sigma(x,y,z)\cdot\vec{\nabla}\Phi(x,y,z)+\sigma(x,y,z)\nabla\cdot\Phi^2(x,y,z) = \frac{\partial}{\partial t}\,\delta(x_s)\delta(y_s)\delta(z_s)$$

where $\nabla^2 = \frac{\partial^2}{\partial x^2} + \frac{\partial^2}{\partial y^2} + \frac{\partial^2}{\partial z^2}$ = Laplacian operator.

Assuming constant conductivity in the direction of y, i.e in the direction of the strike, then the potential derivative of the conductivity with respect to y will be zero. Then equation 3.4 reduces to

$$-\vec{\nabla}\cdot\left[\sigma(x,z)\cdot\vec{\nabla}\cdot\Phi(x,y,z))\right] = \frac{\partial q}{\partial t}\,\delta(x_s)\delta(y_s)\delta(z_s) \qquad \text{eq. 3.11}$$

To solve equation 3.11 it is necessary to use Fourier transform in space (x,k_y,z) by transforming y into the k_y domain. The transformed form of equation 3.11 is

$$-\vec{\nabla}\cdot\left[\sigma(x,z)\cdot\vec{\nabla}\tilde{\Phi}(x,k_y,z)\right] + k_y^2\sigma(x,z)\cdot\tilde{\Phi}(x,k_y,z)$$

$$= Q\delta(x_s)\delta(z_s) \qquad \text{eq. 3.12}$$

where $\Phi(x,y,z)$ is the two dimensional transformed potential and $Q(x,y,z)$ is the constant steady state current density in (x,k_y,z) space. The current density Q can be related to the current I injected at (x_s,z_s) by

$$\tilde{Q} = \frac{I}{2\Delta A}$$

where ΔA is a representative area in the X-Z plane around the current source at (x_s,z_s).

By the finite difference method using an area descretization the solution of $\Phi(x,k_y,z)$ in eq. 3.12 can be obtained in a grid. Applying the following boundary conditions, i.e continuity of the potential across the boundaries and continuity of the current density across the boundaries the finite difference equation is formulated. Then the equation becomes

$$\sum \alpha_{ij}(k_y)\cdot\tilde{\Phi}_{i,j}(k_y) = \frac{I}{2}\cdot\delta(x_s)\delta(z_s) \qquad \text{eq. 3.13}$$

where $\alpha i,j$ is the coupling coefficients.

The computer program developed by Dey and Morrisson (1976) calculates the solution of equation 3.13 for certain filter values and given models, at a certain positionof the current source points. The apparent resistivity value will be obtained by getting the value of the potential after the inverse Fourier transformation.

The rectangular grid system used by Dey (1976) has a grid of 113 nodes in the X direction and 16 in the Z direction. They used a total of 1808 nodes and 23 transmitting point sources to explain the program with the help of specific examples. The grids are denser and equally spaced at the center of the soundings. As the distance increases from the center the spacing of the grids increases. Similarly the vertical resolution of the nodes distribution are fine near the surface and become coarse further to the infinite depth. The advantage of such grid system is to simulate the infinite extent subsurface layers in both the direction of X and Z. Each cell in the grid is defined by a unit length. The unit lengths can be changed according to the desire of the user.

3.5 Discussion

In general the procedure of two dimensional modelling is dividing the earth into reasonable blocks with corresponding values of resistivity. One dimensional interpretations and pseudo-sections of the apparent resistivity values are used to begin the modelling.In order to recognize the distorted part of the sounding, concideration of the areal situation, and the vertical boundary adjustment must be considered. The Schlumberger apparent resistivity at different electrode spacings is calculated and compared with the measured value of the field data. Repetitious changes of parameters of each block and calcula tions are done until a reasonable fit is found. The maximum electrode spacing used in the modelling was 2300 m and for each sounding the model boundaries were defined about this distance. The unit length used was 50 m. Fig 3.3 shows the

results of both the calculated and the measured apparent resistivity pseudo-sections of line 9 from Lake Abaya, Ethiopia.

Fig 3.4 shows the results of a two dimensional model and the resistivity cross-section along line 9. Ten soundings are located along the line with east west orientation. Picket 0.0 is on the ridge of the fault on the edge of the plain. Soundings 1.0E, 2.0E and 3.0E are within the sedimentary zone whereas the rest of the soundings are outside the sedimentary area. Sounding 0.5W was the most difficult one to fit. Inserting a low resistivity block (2.0 ohmm) between 0.5W and 1.0W it was found to lower the high resistivity value of the upper layer. Overall elimination of the high resistivity value at the top creates a problem for the last branch of the sounding and a simple descending curve is obtained. In doing so the thin low resistivity also affects the previous good result of 1.0W. However, the problem is managable, i.e increasing the uppermost layer resistivity until it agrees with the field data. Soundings to the west of 0.5W have more or less comparable resistivity contrasts in all of their corresponding layers. The adjustment of the situation is gained by giving comparable resistivity values and thicknesses, and also by reducing width of the blocks in 3.0W and 1.5W. This brings a rise in the calculated value of the theoretical curve to agree with the field data. Comparable resistivity value of 0.5W as to the soundings to the west of it gives distortion in the regular fit found for sounding 1.0E. Succesful agreement was found with assumed parameters and the field data for soundings 1.0E ,2.0E and 3.0E. By adding a thin low resistivity block in between 0.5W and 1.0E the problem of 0.5 is treated, but it creates a tremendous decrease in the value of 1.0E and a kind of a straight line flanked at both ends. This is because as the electrodes are going further, the current density accummulates within the two low resistivity bodies and constant potential values are obtained. A block of too low resistivity in between high resistivity layers causes a V-shaped curve. The more complicated the model is the more distorted the fit and it becomes difficult to improve it in a short computer time.

The resistivity of the saline sediments along this line within the Abaya plain ranges from 3 to 5 ohmm. The thickness of the sediments is not more than 50 meters. The thickness of the sediments increases towards the west until it reaches the fault line. Prior to this study, the substratum below the sediment was belived to be a part of the upper layer on the western side of the fault. However, the resistivity of the upper layer in the western part is higher than that of the expected comparable layer. This could, however, be the effect of a water from a nearby lake percolating through the loose sediments and depending on the permeability of the rock, accumulating in pore spaces within the rock. This accounts for the lower resistivity value of the rock beneath the sediments than the one which outcrops to the west of the fault. The upper part of the rockformation to the west of the fault, was no permanent water supply which could result in high resistivity values. The second reason could be, that the thickness of this expected layer may be small, so that it could be masked by the dominant thick layers above and below it. Because of its small thickness it might not be detectable and could be generalised into the second, geophysically classified layer.

3.6 Conclusions

The integration of both one and two dimensional modelling contributes to the improvement of the exact interpretation of Schlumberger soundings. The thin low resistivity (3-5 ohmm) layer on the surface of the lowland east of picket 0.0 is correlated with the fluvial deposits. The thickness of these sediments is not more than 50m. The resistivity of the substratum below the sediments ranges from 10 ohmm to 40 ohmm.

There is a good sequence of characteristic layers to the west of the main fault or picket 0.0 outside the sediment area. From the present work it is possible to infer these characteristic layers as follows:

- high resistivity zone (greater than 50 ohmm)about 50 - 200m thick. But this is not found underneath the sediments.

- an intermidate resistivity layer (10 - 50 ohmm) about 200 - 400m thick. There is good contrast of this layer to the eastern side underneath the sediments.

- layer overlain by the sediments. But this low resistivity layer seems to picket 1.0E and 3.0E there is a similar low resistivity block below the second layer overlain by the sediments. But this low resistivity seems to be blocked by relatively higher resistivity block below 1.0E.

- high resistivity bottom layer.

The low resistivity anomally along this line closes around picket 0.5W and appears to continue upward vertically according to the pseudo-sections. As to the two dimensional model and the resistivity cross-section the low resistivity zone of this area could indicate thermal fluid zone along the fault line in an agreement with the pseudo-sections. Extension of the low resistivity zone towards the east is limitted, this may indicate the none existance of thermal actvities towards the east. There seems to be an intermidate resistivity body under the second layer of 1.0E.

4 THE LAKE ABAYA GEOTHERMAL AREA

The Lake Abaya region is one of many geothermal areas in the lakes district that extends from Lake Shamo in the south up to the Awash river watershed. The area is considered to be one of the important prospect areas (UNDP 1973) in relation to the geochemically inferred high reservoir temperature of 177 - 265°C.

The area has been considered geologically, geochemically and geophysically in many reports, e.g Demissie G. (1980), GENZL (1980), Abakoyas J. (1980), Tezcan, et al. (1983).

4.1 Geology of the study area

Lake Abaya is located 6°15N, 37°55E within the Lakes District at an altitude of 1170 m above sea level. It occupies a tectonic depression in the rift floor. The area northwest of Lake Abaya is dissected by NNE trending fault swarms in an en-echelon manner. Aligned scoria cones mark a basaltic eruption from the surrounding fault zones. The youngest faults form small horsts and grabens within the basalts. Towards the lake the basalts are thin. The western and northern part of the study area is mainly covered by the Abela basalts of the Holocene period. The eastern part is masked by lakustrine sediments, deltaic and fluvial deposits. The geological map of the area is shown in Fig. 4.1

Rhyolite outcrops of Holocene age are found about 15 to 20 km north of the study area. The expected strategraphic formations of Abela basalts are pliocene Chewkare-ignim-brite and peralkali-rhyolites. These outcrops can be seen on the immediate western edge of the Lake Abaya associated with the great Chewkare fault with SSW-NNE extention in the form of narrow ribbon. Generally the most active and important hot springs of the prospect area emerge from the same fault alignment starting from the northwestern shore of the lake up to the middle of Chewkare fault. The Humbo-Guroucha basalts, which are considered to be of the same age, outcrop about 20km west of the survey area. Aiba basalt or Trap basalts cover the plateau and also

occur in the rift floor, outcroping at 15 - 20 km SW of the prospect area. In the surveyed area this formation is expected to underlie the above ones with pre-camberian gneis basement.

4.2 Geothermal manifestations

Thermal manifestations observed in the area are; one strongly discharging fumarole associated with a boiling hot spring (95°C) and other warm and hot (42 -67°C) springs. All of them are situated on an alignment of the Chewkare fault and also associated with the ignimbrites extending from SSW to NNE on the northern edge of the Lake Abaya. Near the northern shore of the lake there are hot springs within the course of one branch of the Bilate river. Just at the mouth of the river, near the fault, these hot springs represent seasonal geysers. Especially during wet seasons these geysers start to splash water with a turbulent sound at regular time intervals. The fault ridge bordering the north west tip of the lake has a horst form with an arrowlike shape pointing NNE. Both sides of the ridge are altered. However the eastern side is more altered than the western one, with sulphur deposits and silica preciptation. Fumaroles with a small discharge and paths of hot ground (500 m^2) at boiling temperature are situated 10 - 12 km north of the geophysically surveyd area and associated with rhyolite outcrops (UNDP, 1973).

The geochemical analyses of hot springs in the Abaya area are described in the UNDP (1973) techinical report and the following information is taken from there. The location of hot springs is shown in Appendix II.

The temperature of springs 17, 8, 15 and 16 ranges from 37 to 65.5°C. Except for 17, the springs evolve CO_2 which increases the pH near the surface and results in limonite deposition. The discharges of the springs are high and they are heated either by rock conduction or by steam injection into shallow waters. The high CO_2 discharge also suggests a shallow origin.

Spring 6, however, is boiling. It deposits some siliceous sinter,and has a comparatively high Cl content Geochemical thermometers suggest high underground temperature. The silica content which is the highest for the Lake District, suggests a quartz equilibrium temperature of about 177°C. This value may, however, be affected by the high pH value. Underground temperatures based on the Na/K geothermometers are of the order of 265°C. This water is probably representative of deeper water underlying the area. Steam is librated and ascends, heating perched groundwater, which probably is the source of surrounding cooler springs. There is evidence from old travertine deposits that activity of Chewkare, particularly in the north was once more extensive, and possibly more intensive. The apparent decrease in activity may have resulted from calcite blockage of feeding fissures near the surface and this may inhibit the flow of deep chloride water to the surface. The high bicarbonate content suggests high CO_2 concentrations. Hence calcite will tend to deposit as steam separates from the ascending water column, and could also cause scaling problems in production wells.

4.3 Geophysical survey

The area has been studied extensively using most of the geophysical methods that are useful for prospect exploration. Dipole - dipole resistivity survey and Schlumberger electrical soundings have been carried out and interpreted since 1980. The description here is based on the results obtained from both one and two dimensional interpretation of selected soundings of the area.

The anomalous area was surveyed by east-westerly oriented and extended lines. The location map is given in Appendex I. The interval between profiles is 700 m and the distance between consequent VES points is 500 m to 1000 m. Self-potential measurements were made along profiles 9, 15 and 17. Gravity surveys were made along all the lines and in the surrounding roads and previous lines of reconnesance survey were taken.

The resistivity sections and two dimensional interpretation results of line 9 are explained in Chapter 3. The results of the self-potential measurements have been described by Tezcan et al. (1983). Due to shortage of time the gravity data have not yet been computerized and not modelled. However, the Bouguer gravity anomaly profiles are presented in some lines. From these profiles there is no clear indication of density differences between the eastern and western side of the fault.

All the profilesare interpreted two dimensionally except profile 16. Fig. 4.2 shows measured and calculated resistivity pseudo-sections along line 15. According to the Figure there exist a low resistivity closer around pickets 0.1W and 0.5E. Fig. 4.3 shows two dimensional model and resistivity section of line 15. A block at a shallow depth around pickets 0.1W and 0.5E is observed. It extends to the west and is relatively deeper under the rest of the pickets (0.5W, 1.0W, 2.2W and 3.0W).

Line 17 is 1.4 km north of line 15 with the same orientation. Fig. 4.4 shows calculated and measured resistivity pseudo-sections of line 17. There is a low resistiviy encloser around picket 1.0E. This picket is within the sedimentary zone but close to the fault. The two dimensional result and its resistivity section is shown in Fig. 4.5. There are four characteristics layers both to the east and to the west of the fault. Some changes are seen in the resistivity contrast along the line. However, there is nearly the same contrast in all the blocks along the low resistivity zone.

Line 14 is 700 m south of line 9 with the same orientation. Four soundings were measured along this line and in Fig. 4.6 both measured and calculated resistivity pseudo-sections are shown. The pseudo-section show a low resistivity encloser tendency to the east i.e. to the fault and the lake. But the two soundings to the east i.e. picket 0.5W and 1.0W are shallower. Because of areal difficulty the maximum AB/2 used for the soundings is 1km, whereas, for the two dimensional interpretation the maximum elec trode distance is defined to be 2300 m. Because of this there is a slight varation in the two

pseudo-sections under these pickets. The two dimensional result is given in Fig. 4.7. All the threesoundings shows three layers characteristics except that picket 2.1W is four layers. However, the low resistivity layer seems at shallower depth under pickets 0.5W and 1.0W.

The overall layering characteristics of each line to the west of the fault, are the same as that of line 9. Along the profiles to the west of the fault almost all the soundings show the following characteristics layers:

- a high resistivity layer; - an intermidate resistivity layer; - a low resistivity layer; - a high resistivity bottom layer.

In most cases the resistivity values are comparable. It is therefore possible to correlate the first high resistivity layer with the dry and/or consolidated part of the basalts in the area. The intermidiate resistivity layer can be correlated with the ignimbrite zone, and the low resistivity layer with the rhyolite and it's altered products. The most likely statigraphic correlation of the bottom high resistivity layer is to the Precambrian gneiss underlying the trap basalts.

Generally pickets 0.0 on line 9, and pickets 0.5E, 0.1 W on line 15 show a low resistivity zone outcropping vertically around them. These pickets are situated nearby the major fault, where the main thermal manifestations are located.

The two dimensional modelling suggests that the upper high resistivity layer has a variable thickness of 50-200 m. The second layer has a thickness in the range 200-400 m. The thickest layer in all the profiles is the low resistivity zone. Its thickness seems to increase in the areas of low resistivity outcrops and enclosures explained above. The low resistivity zone seems shallower in these areas.

4.4 Geothermal model of the Lake Abaya area

Tezcan, et al. (1983) describe the low resistivity anomaly of the studied area as small, unique and very conspicious. This discription is based on the result of the measured resistivity pseudo-sections and one dimensional interpretation. These results are now confirmed by two dimensional interpretation. A good correspondance of the thermal manifestations and the low resistivity enclosures around the major fault is observed. The vertical low resistivity enclosures along line 9 and line 15 coincide with the Chewkare fault belt. This may indicate that the thermal activity is mainly restricted to the fault zone. Geochemical analyses of the hot springs suggest underground temperature of 170-260°C possibly representing geothermal water underlying the Chewkare area. According to the geophysical result the low resistivity structure may be due to the interaction of geothermal waters within the low resistivity layer. These waters may be heated by young volcanic intrusions or dyke along the opening of the fault. Their interaction with the surrounding rocks causes the appearance of these low resistivity anomaly zone. The anomaly itself can be pourous and probably permeable medium filled by these waters. The horizontal low resistivity extention to the west may be the continuation of the fluid along permeable medium, where the Chewkare area is the main upflow zone.

4.5 Conclusions

Schlumberger soundings from Lake Abaya geothermal area have been modelled two dimensionally. The four profiles that are interpreted here suggest that the Chewkare fault zone is the most promising low resistivity area. According to the distribution of the main thermal manifestations. Consideration of line 9 and 15 is necessary. The thick low resistivity block under pickets 0.5W and 1.0W is responsible for the vertical low resistivity enclosure in the pseudo-sections of line 9. This block should be the main conduit of the hot springs and the fumaroles including the patches of altered grounds along the faultridge in the area. Similarly, thicker low resistivity blocks under

pickets 0.1W and 0.5E of profile 15 must be responsible for the very low resistivity enclosers in the pseudo-sections. These should be the conduit of the strongly splashing hot spring near picket 0.1W and the alteration of the ground. This situation confirms that these structures are the main causes of the thermal activity in the area. Accordingly, these areas should be the first target for deep drilling. This is not only based on the geophysical result but also the geochemical analyses of the hot springs in the area and the distribution of the thermal manifestations.

An extension of the low resistivity zone towards the west is seen in all the profiles. In order to check this zone in relation to geothermal fluid production shallow temperature gradient wells are necessary. However, prior to any drillingsurface temperature survey that can possibly cross the northern end of the lake, including the total survey area, may give additional information.

ACKNOWLEDGEMENTS

The author is very much indepted to Brynjolfur Eyjolfsson, who supervised the work in this report and for his valueable discussions through out the training time. The author also wishes to express his gratitude to Dr. Ingvar Birgir Fridleifsson for his active part in the coordination of the programme and for reading the manuscript. Greatful acknowledgements are due to Sigurjon Asbjornsson for his continued help during our stay at the university,to all the lecturers at the United Nation University,and to the society of the National Energy Authority (ORKUTOFNUN) of Iceland.

The author is also greatful for the help of Befekadu Oluma (Project Geophysicist in Geothermal Exploration Project in Ethiopia) and Abiy Hunegnaw during the preliminary interpretation as well as for scientific discussion during his work experiences. He is dedicated to thank Ato Getahun Demissie general manager of the Ethiopian Institute of Geological Surveys for his permission to participate in this training programme. Finally, the author would like to thank the geophysics crew of Abaya in 1982 - 1983 for wonderful working time together, in collecting all the data used in this manuscript.

REFERENCES

Abakoyas J., 1980; Preliminary Report on Geophysical Activities in the Central and Southern Lakes Areas (Aje and Abaya Areas) January, 1980.

Dey, A., 1976; Resistivity Modeling for arbitrary shaped two-dimensional structures part users guide to the FORTRAN algorism RESIS2D. LBL-5283.

Dey, A., and Morrison, H.F., 1976; Resistivity modeling for arbitrarily shaped two-dimensional, structures. Geophys. prospect., 27, 106-136.

GENZL, 1980; Lakes District Geothermal Energy Project Report of Technical Review Committee,February 1980, Committee Engaged by Geothermal Energy New Zealand Limited, under contract to United Nations.

Keller, G.V and Frishnet, F.C., 1966; Electrical methods in geophysical prospecting, Pergamon press, New York, 519.

Koefoed, O., 1979; Geosounding Principle1. Resistivity Sounding Measurements. Elsevier, Amsterdam. 276 pp.

Mufti, R.I, 1976; Finite Difference resistivity modeling for arbitrarly shaped two-dimensional structures. Geophysics 41, 62-78.

Tezcan, A.K, Befekadu, O. Abiy, H. and Ketsela, T.1983; Geophysical geoelectrical report of Lake Abaya (Technical report).

UNDP, Technical Report., 1973; Investigation of Geothermal Resources For Power Development Ethiopia, Geology, Geo-chemistry and Hydrology of The East African Rift System Within Ethiopia, Technical Report, UNDP; 1973.

Ward, H.S. and Sill, W.R., 1983; Resistivity, Induced polarization, and Self-Potential Methods in Geothermal Exploration. UNU Geothermal Training Programme, Iceland, Report 1983-3. pp 94.

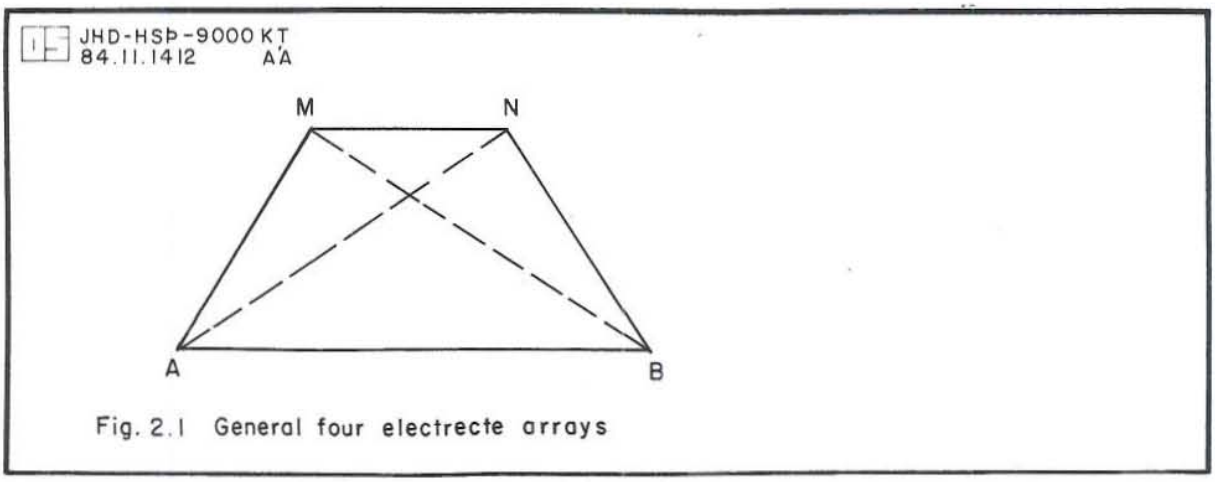

Fig. 2.1 General four electrecte arrays

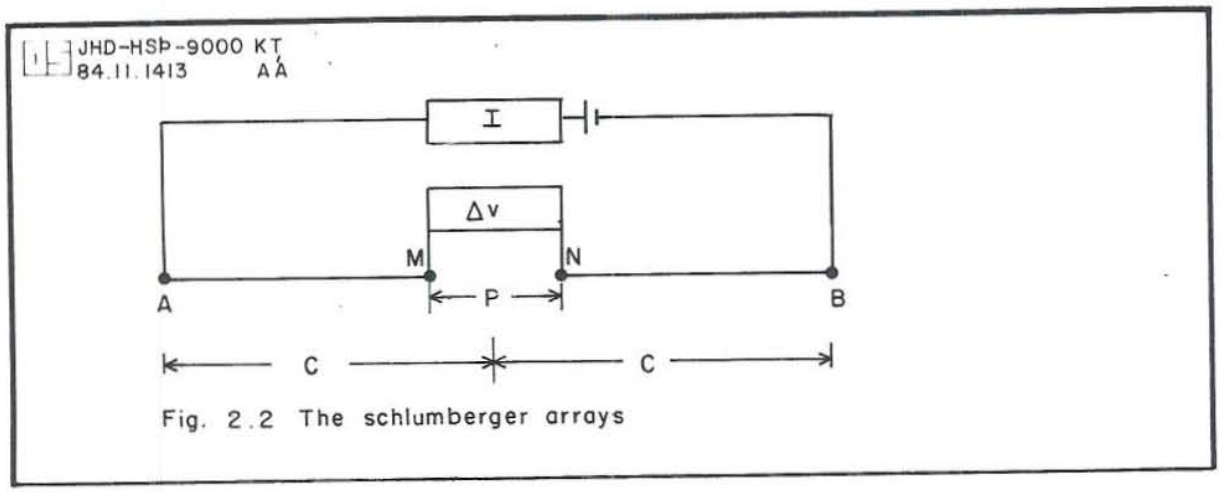

Fig. 2.2 The schlumberger arrays

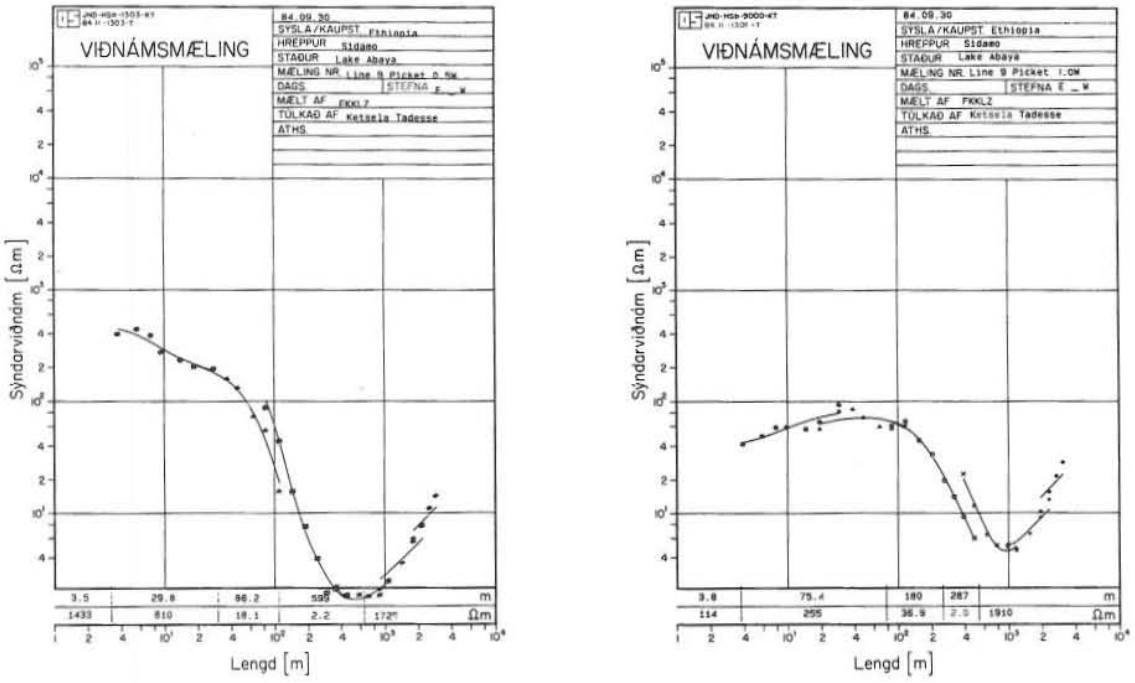

Fig. 3.1 Ellipse fits to soundings 0.5 W and 1.0 W in line 9.

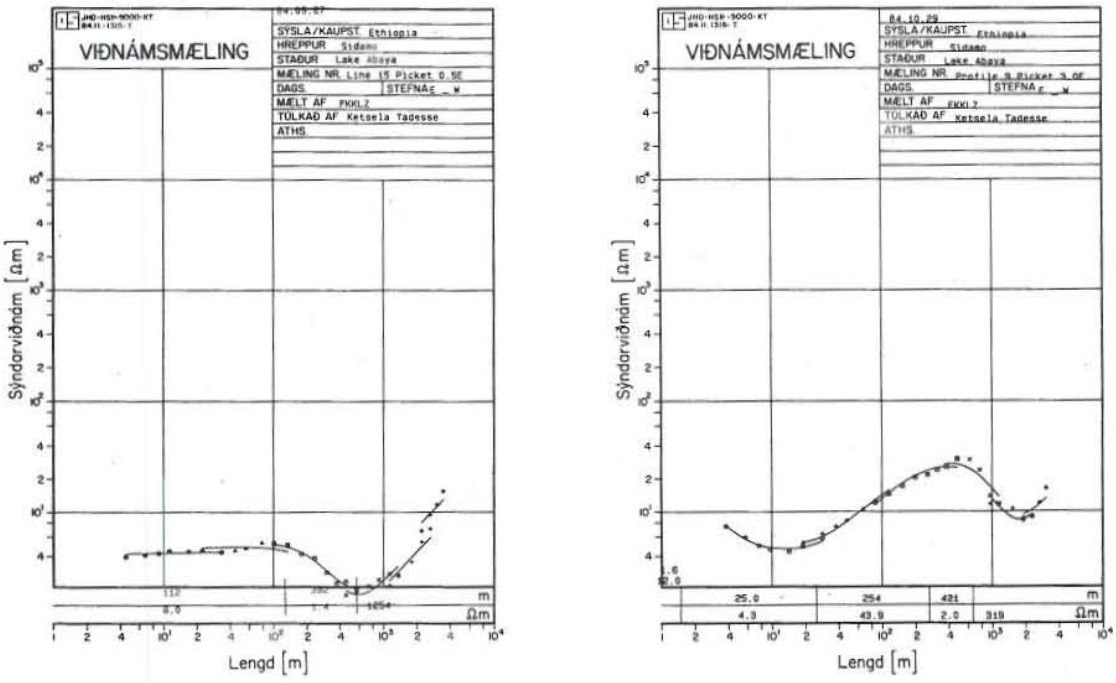

Fig. 3.2 Ellipse fits to sounding 0.5E in line 15 and 3.0E in line 9.

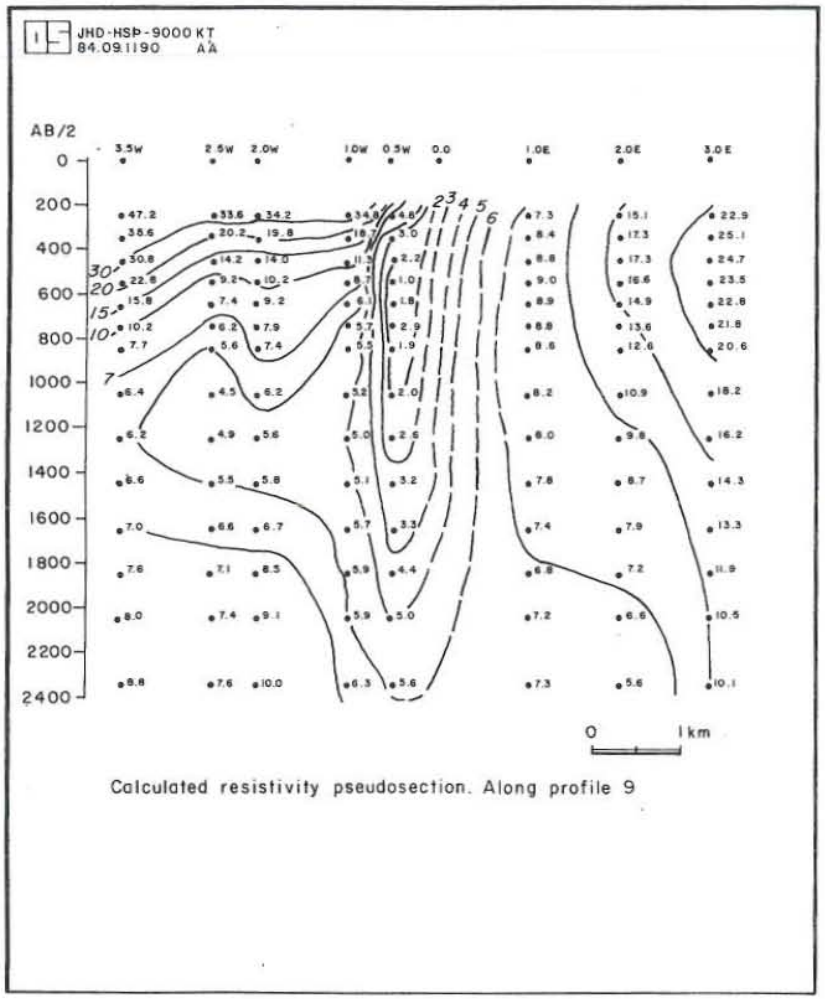

Calculated resistivity pseudosection. Along profile 9

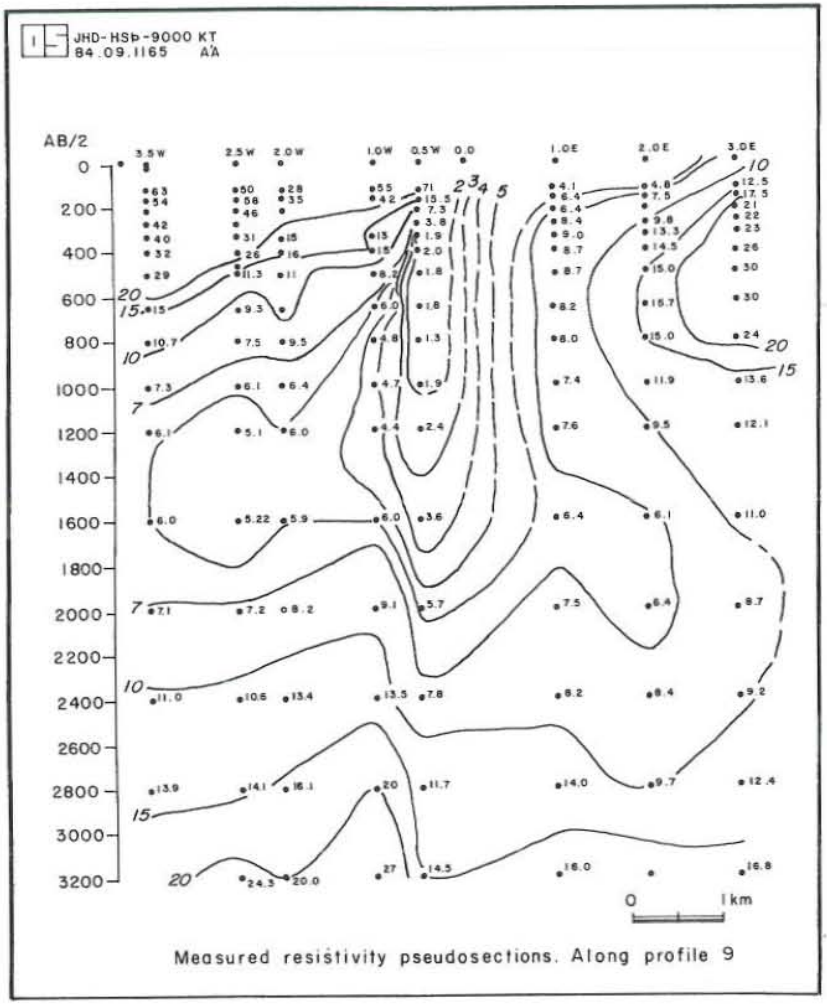

Measured resistivity pseudosections. Along profile 9

Fig. 3.3 Measured and calculated resistivity pseudosections along line 9.

JHD-HSI -9000-KT
84.09. 1154. '0D

Fig. 4. 1.

40

GEOLOGIC MAP OF THE LAKE ABEYA

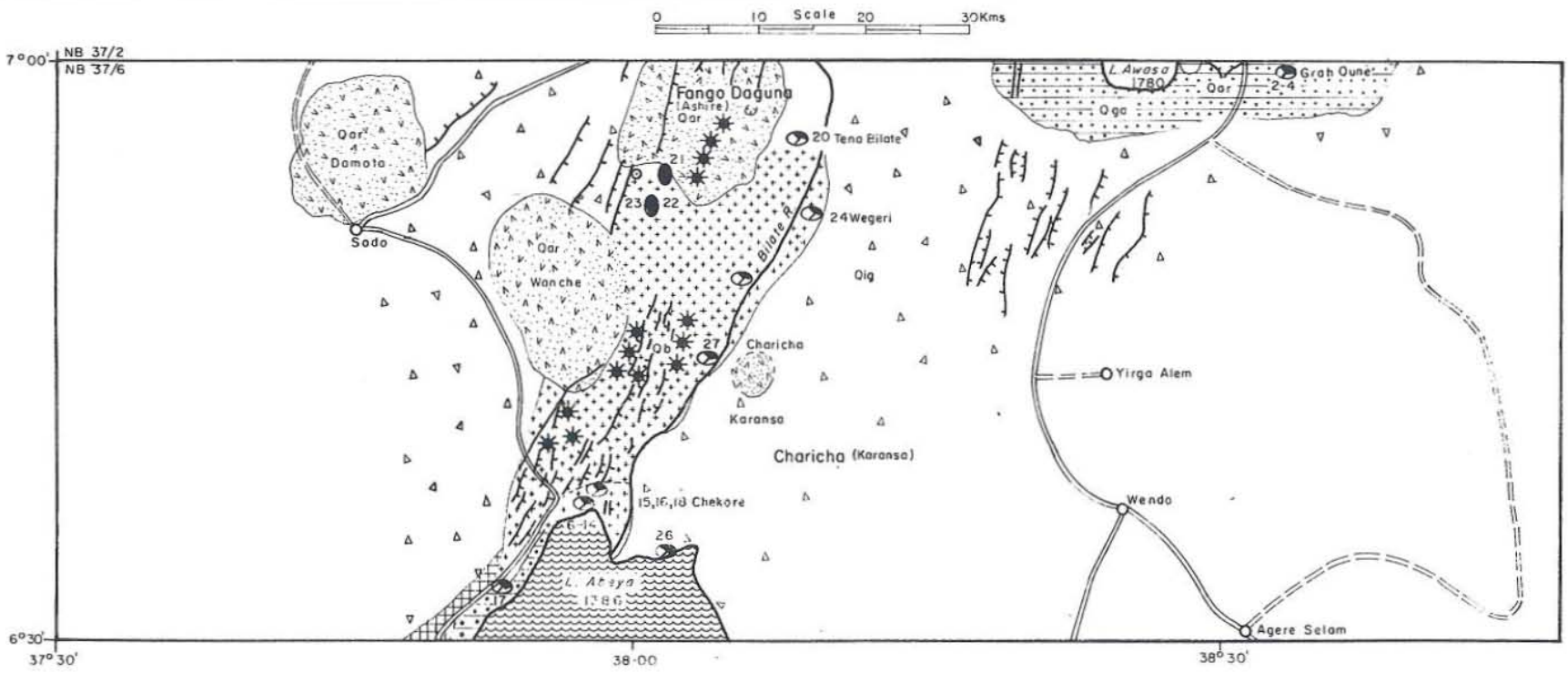

- Fault showing down throw
- Cone
- Crater
- Hot spring with number
- Fumarole with number
- Well sample with number

JHD-HSP-9000-KT
84.09.1188. 'OD

Fig. 3.4.

2-Dimensional model (profile 9)

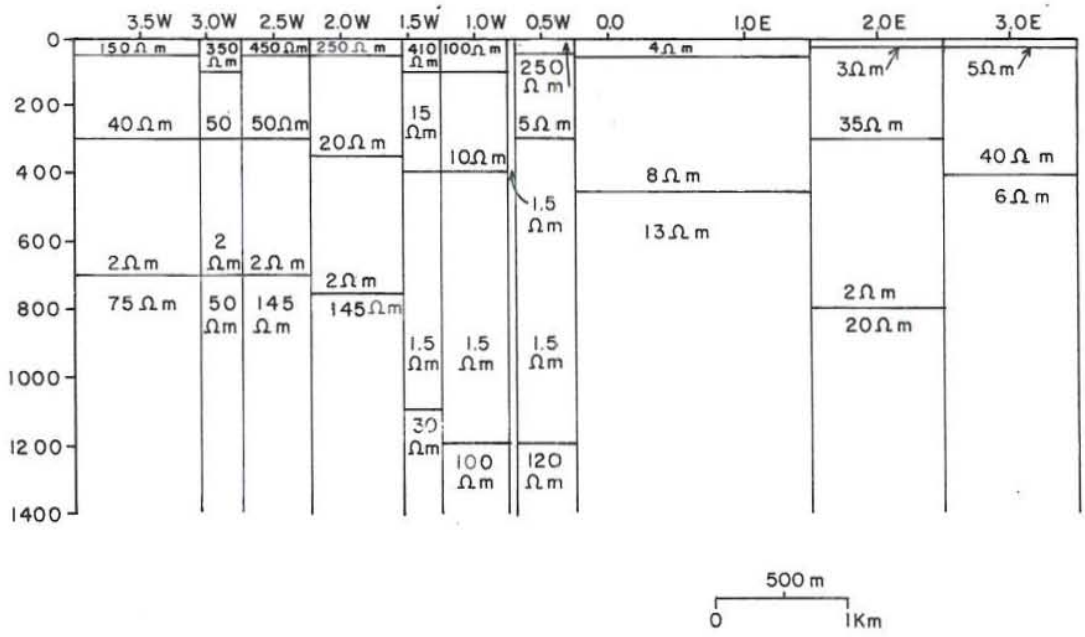

JHD-HSI-9000-KT
84.09.1189 'OD

Fig. 3.4.

Resistivity cross-section along profile 9

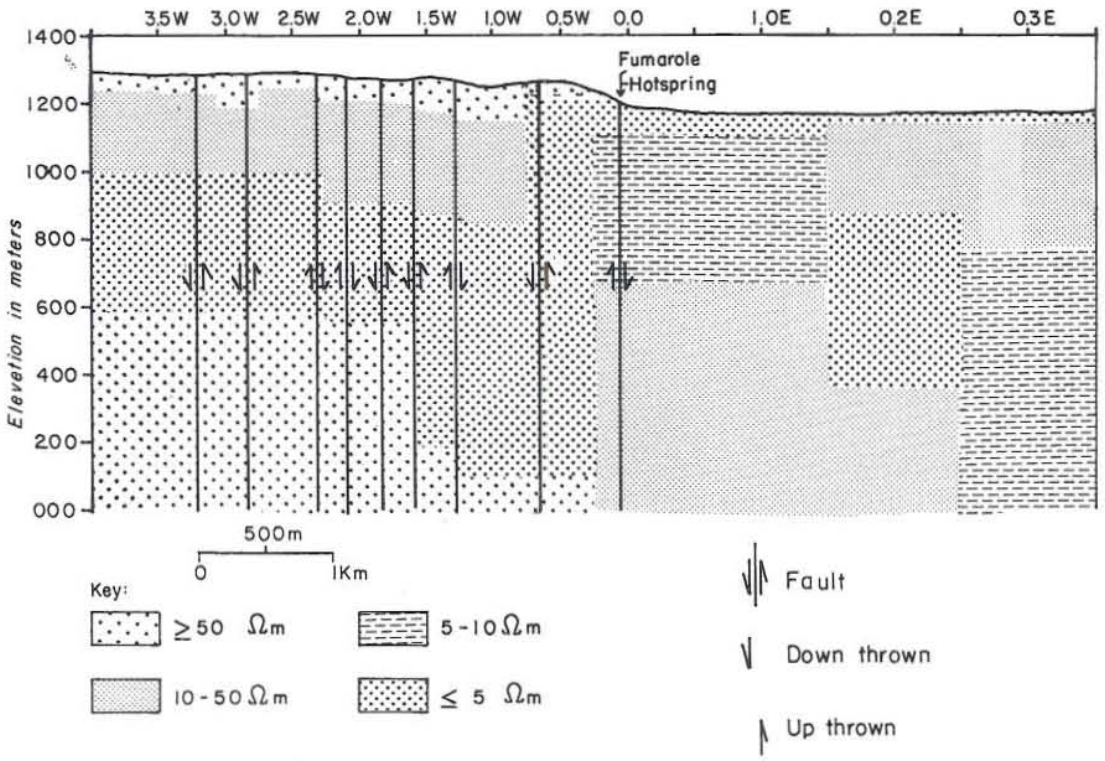

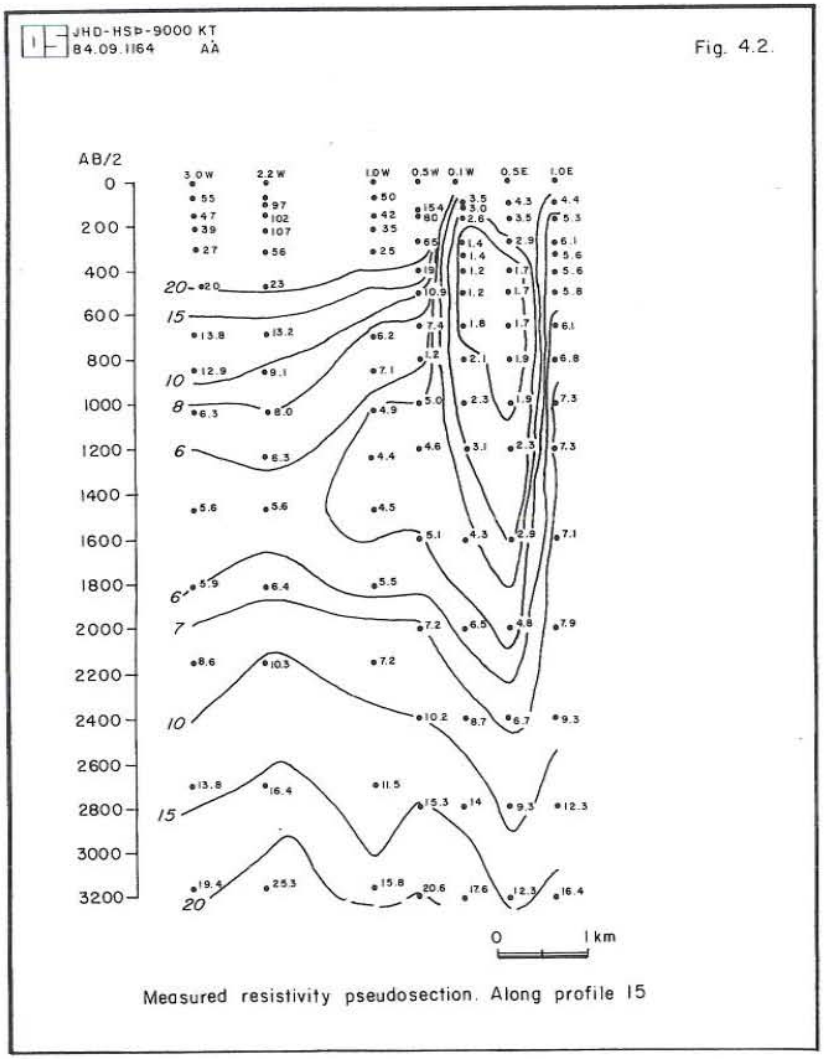

Measured resistivity pseudosection. Along profile 15

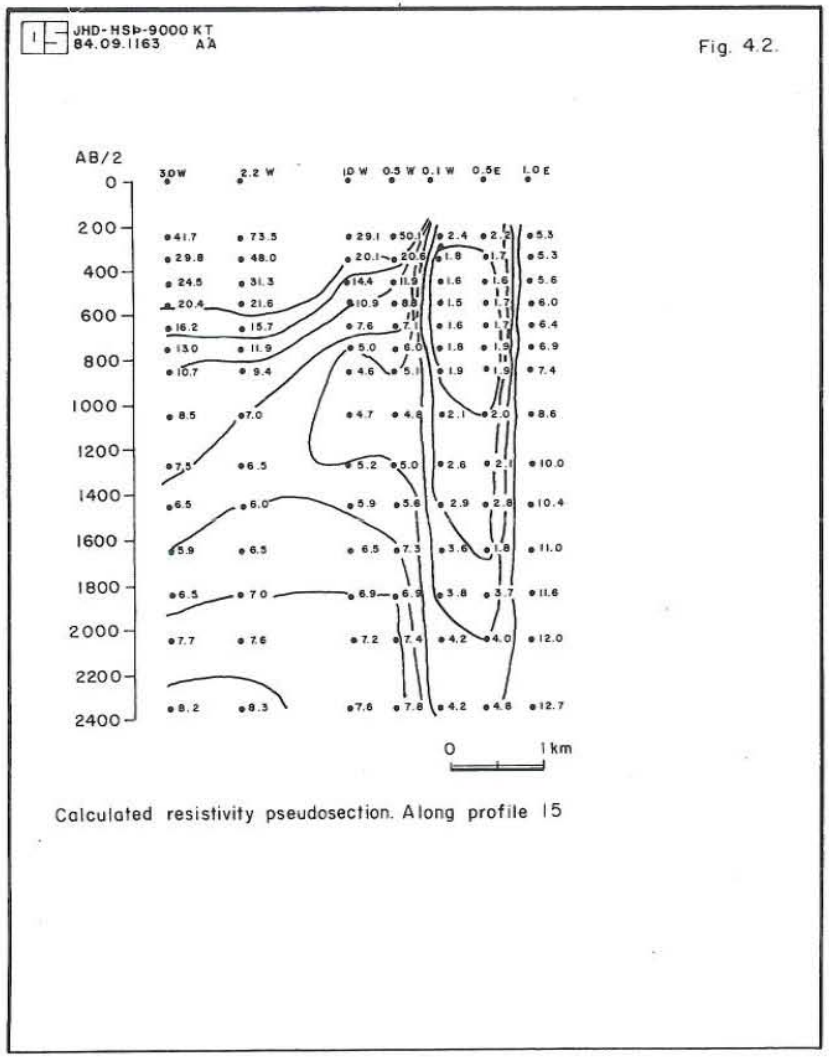

Calculated resistivity pseudosection. Along profile 15

JHD-HSP-9000-KT
84.09.1186. 'OD

Fig. 4.3.

2-Dimensional model (profile 15)

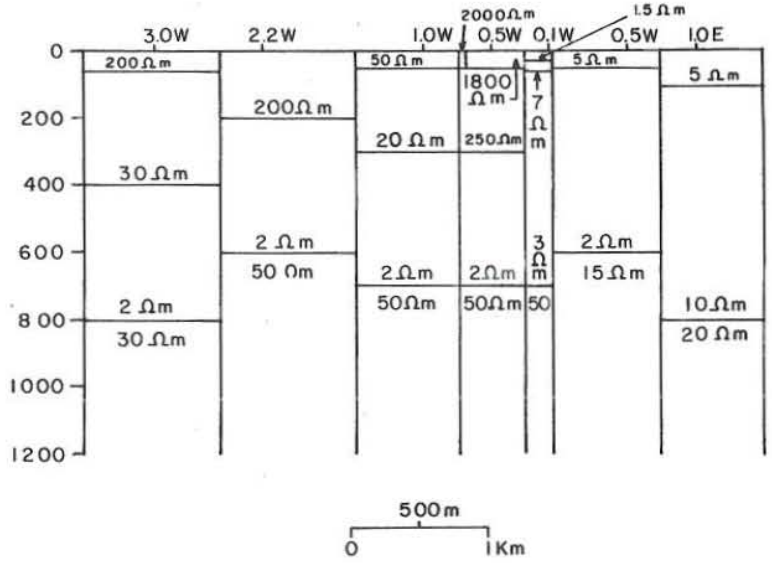

JHD-HSI-9000-KT
84.09.1187. 'OD

Fig. 4.3.

Resisivity cross-sectin along profile 15

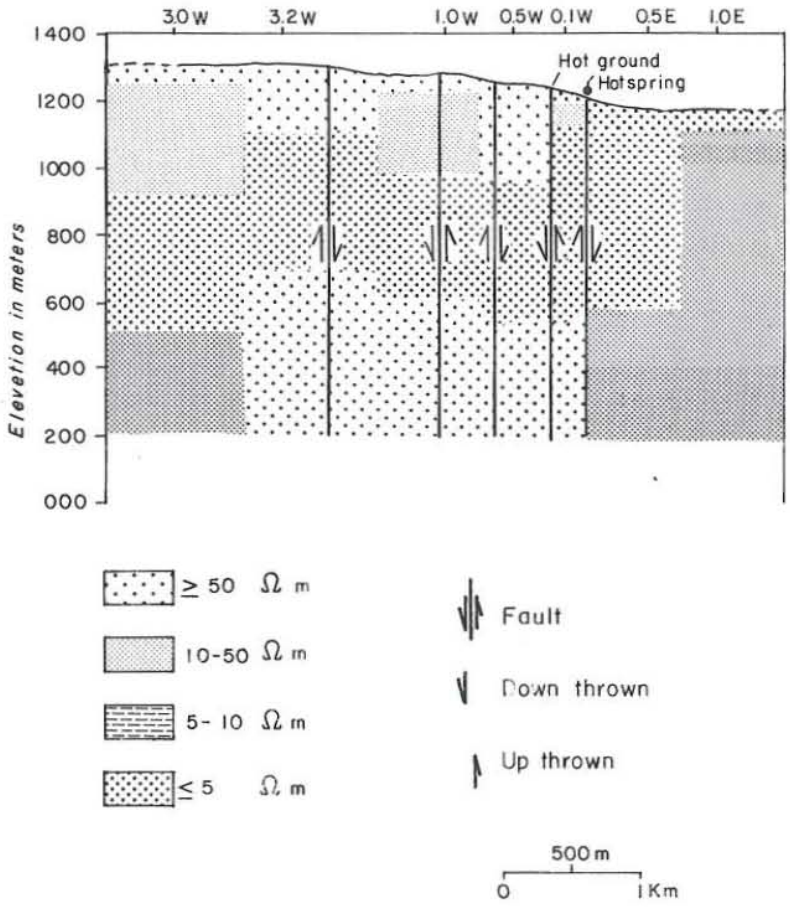

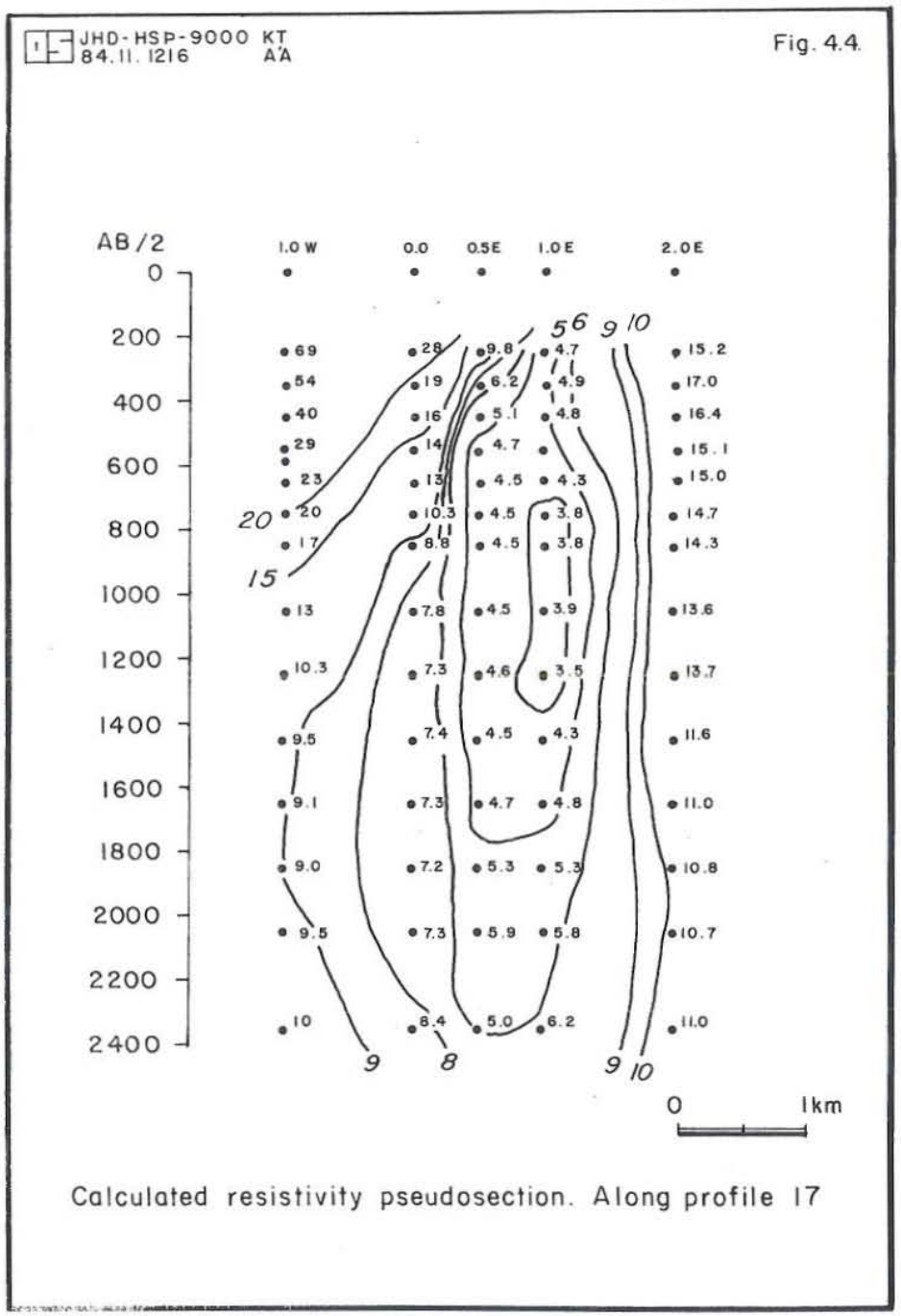

Calculated resistivity pseudosection. Along profile 17

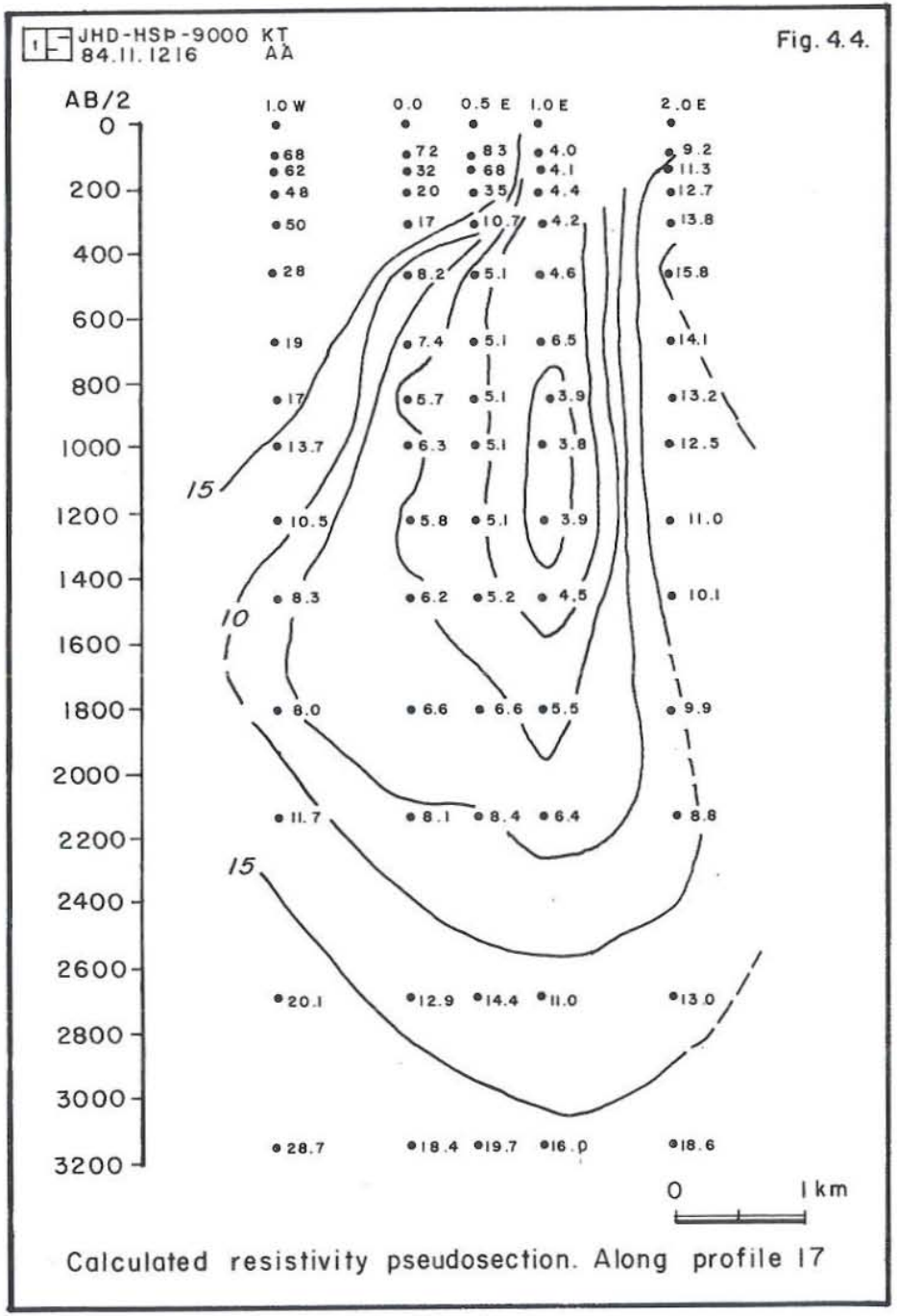

Calculated resistivity pseudosection. Along profile 17

JHD-HSI -9000-KT
84.11.1273 'OD

Fig. 4.5.

Line 17, 2-Dimensional model

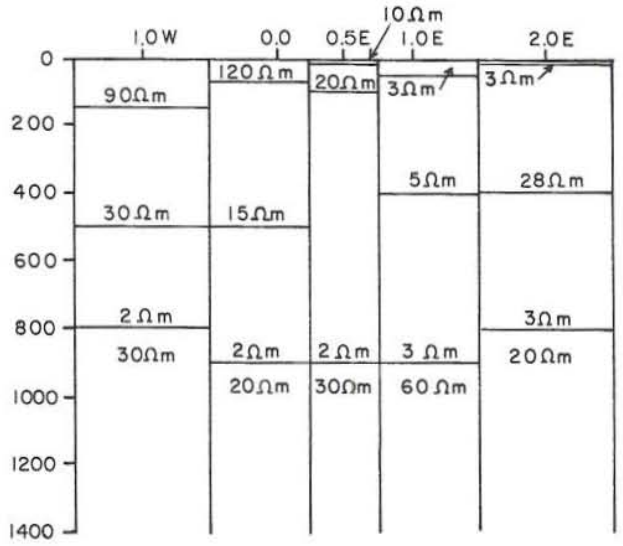

JHD-HSP-9000-KT
84.11.1272 'OD

Fig. 4.5.

Line 17, 2-Dimensional resistivity section

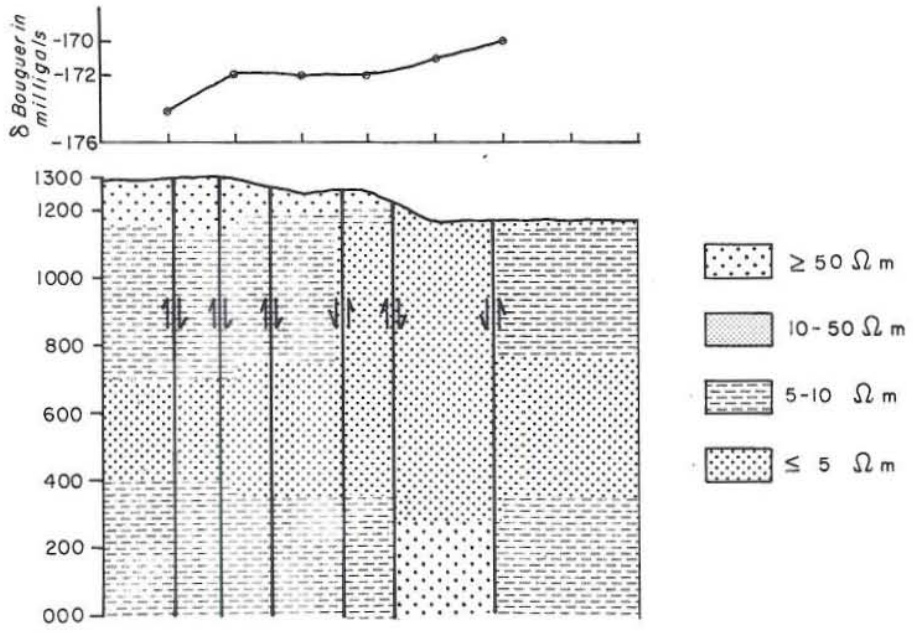

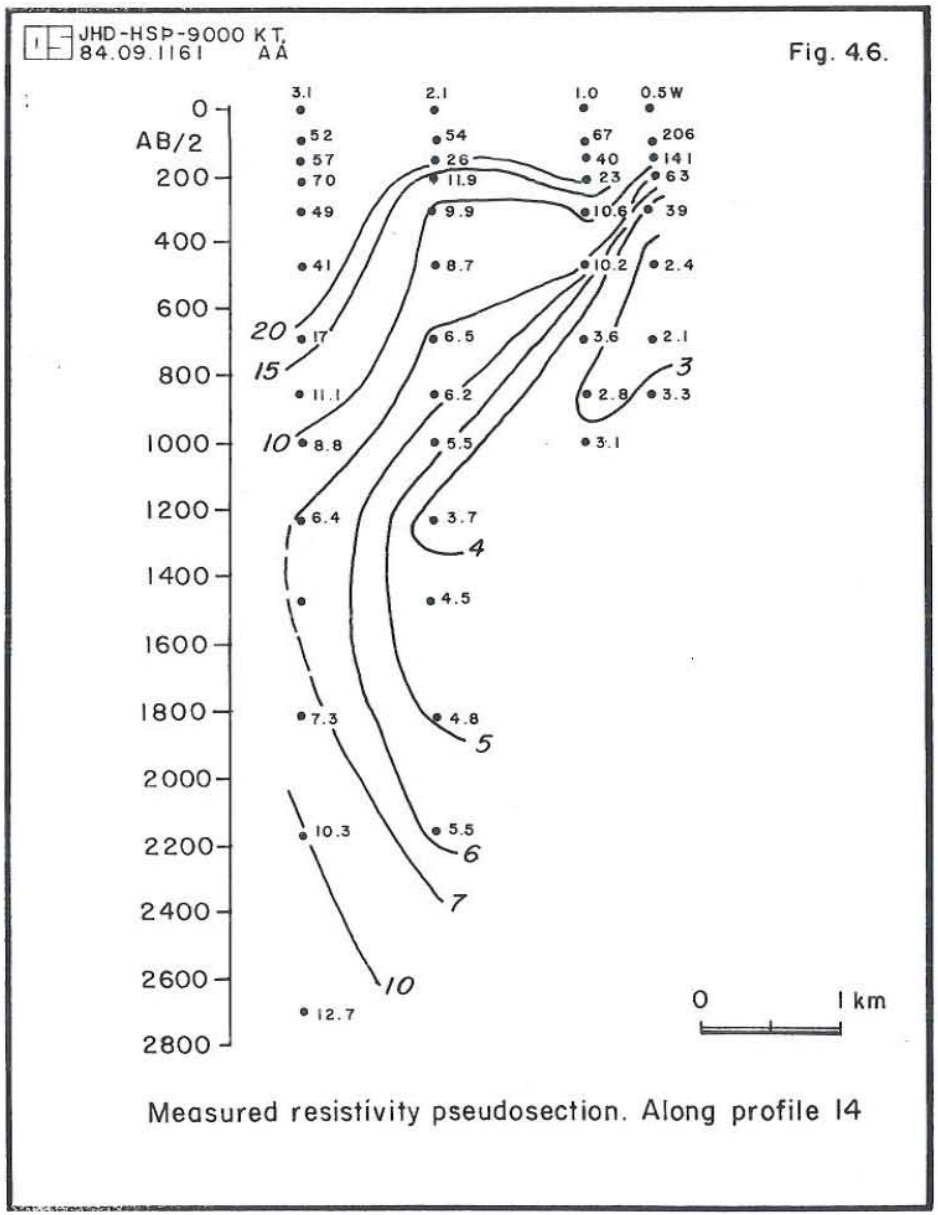

Measured resistivity pseudosection. Along profile 14

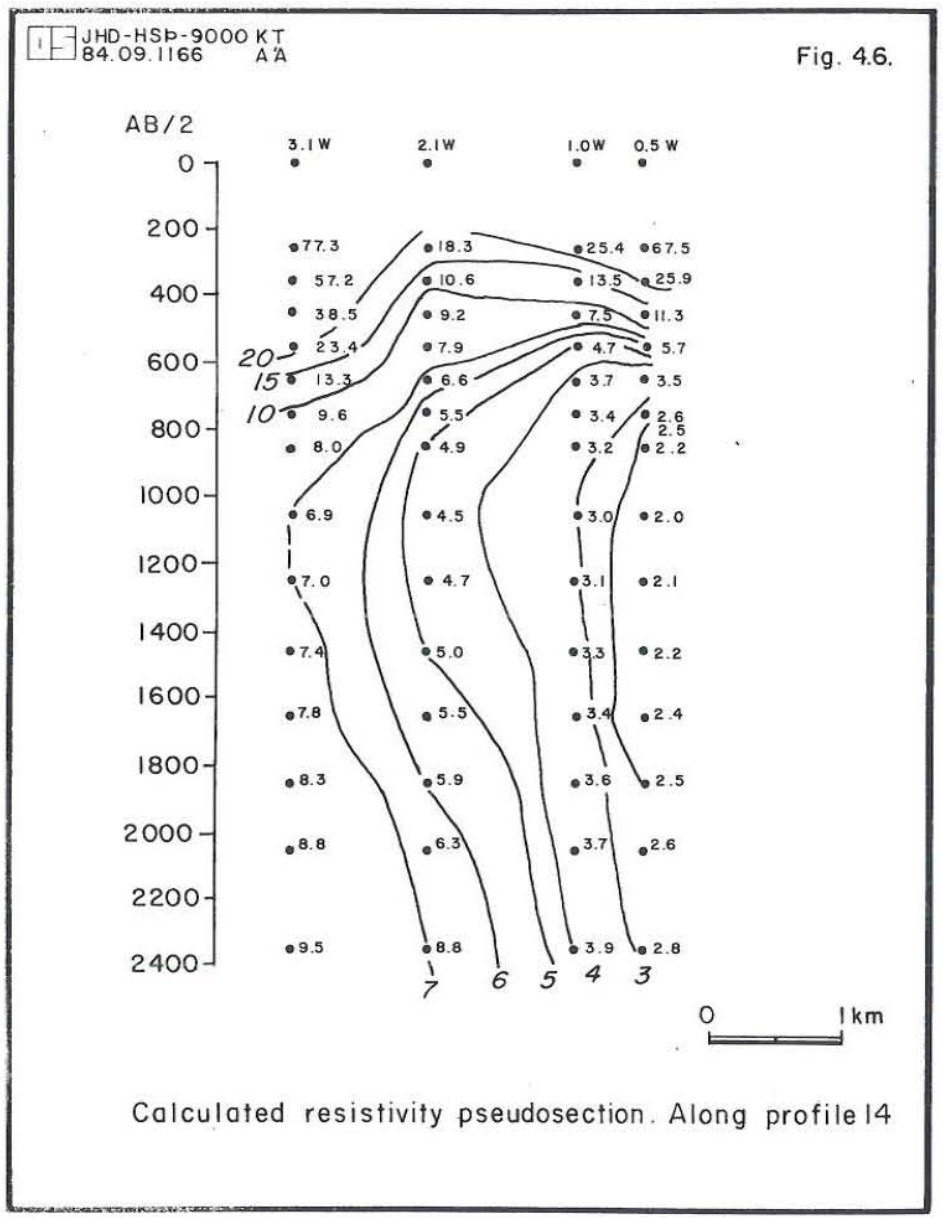

Calculated resistivity pseudosection. Along profile 14

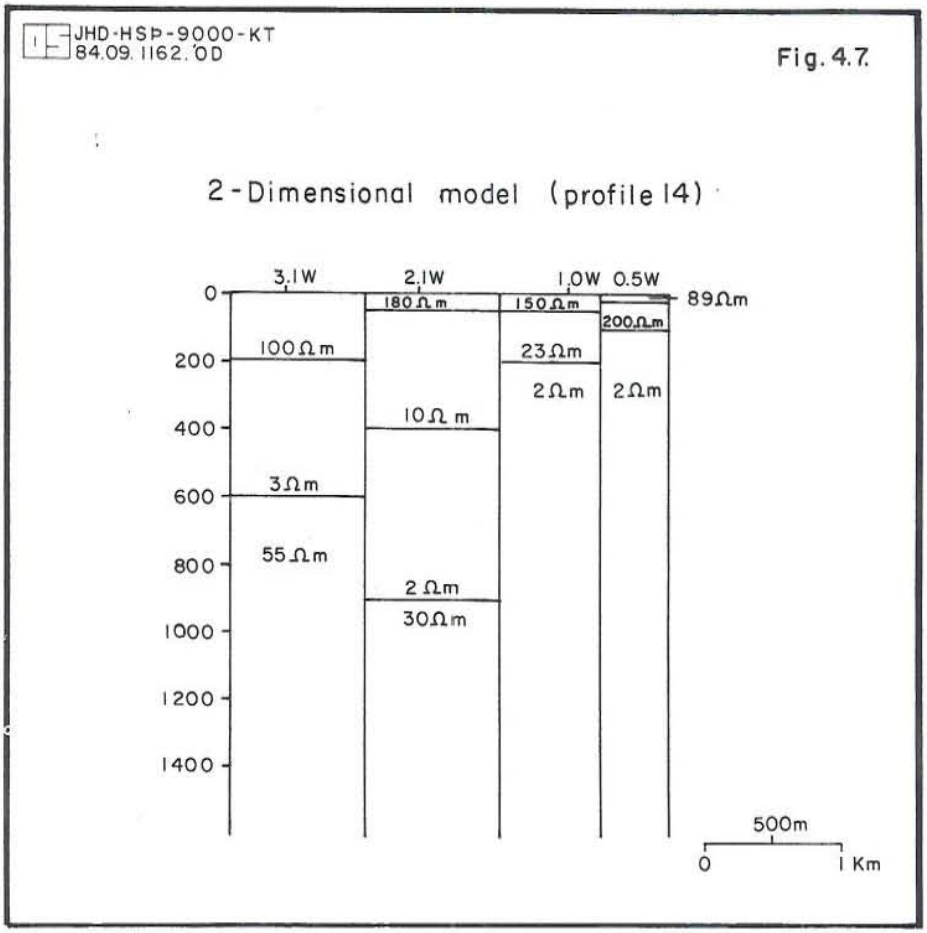
JHD-HSP-9000-KT
84.09.1162.0D
Fig. 4.7
2-Dimensional model (profile 14)
3.1W
2.1W
1.0W 0.5W
0
200
400
600
800
1000
1200
1400
180Ωm
150Ωm
89Ωm
200Ωm
100Ωm
23Ωm
2Ωm
2Ωm
10Ωm
3Ωm
55Ωm
2Ωm
30Ωm
500m
0
1 Km

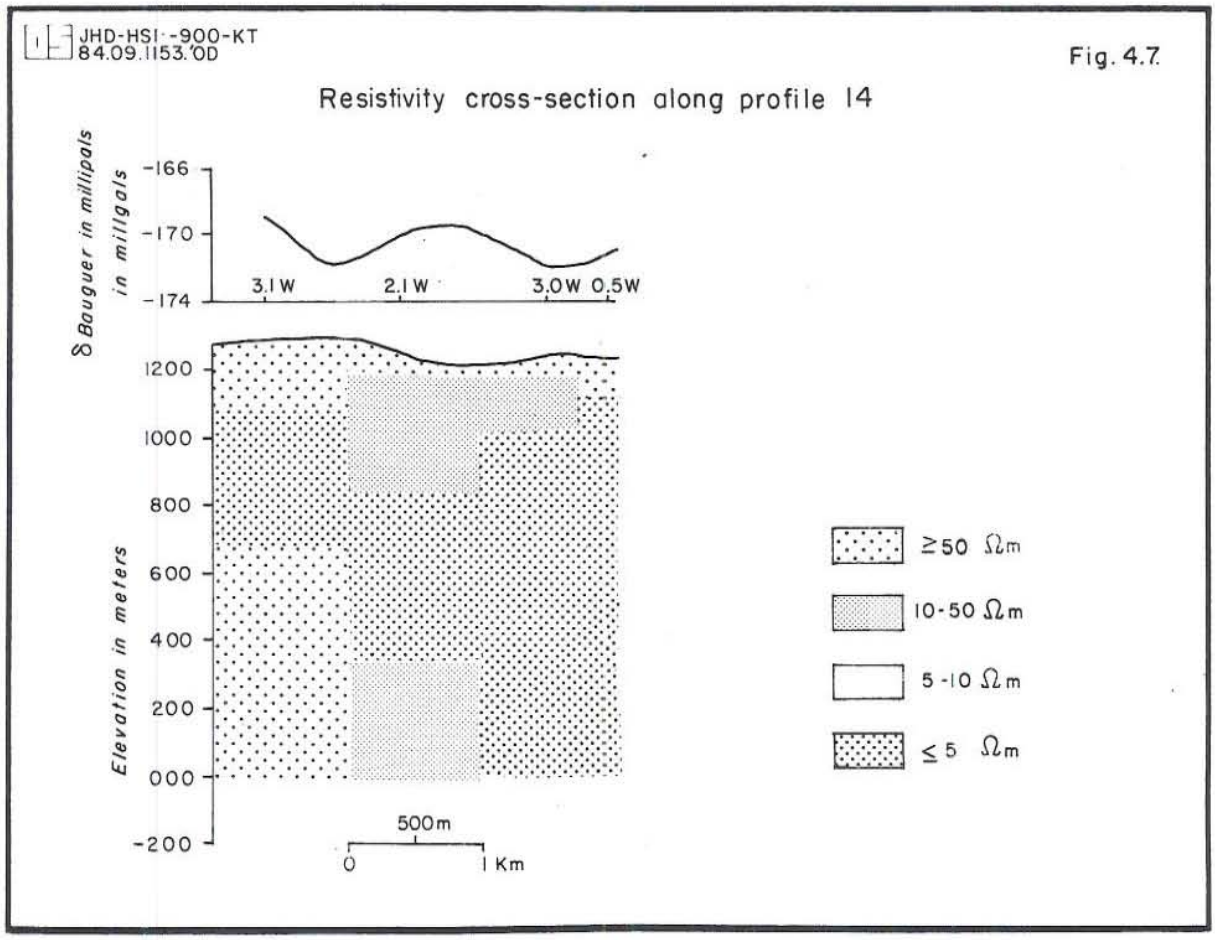
JHD-HSI-900-KT
84.09.1153.0D
Fig. 4.7
Resistivity cross-section along profile 14
δ Bouguer in millgals
-166
-170
-174
3.1W
2.1W
3.0W 0.5W
Elevation in meters
1200
1000
800
600
400
200
000
-200
500m
0
1 Km
≥50 Ωm
10-50 Ωm
5-10 Ωm
≤5 Ωm

APPENDIX I

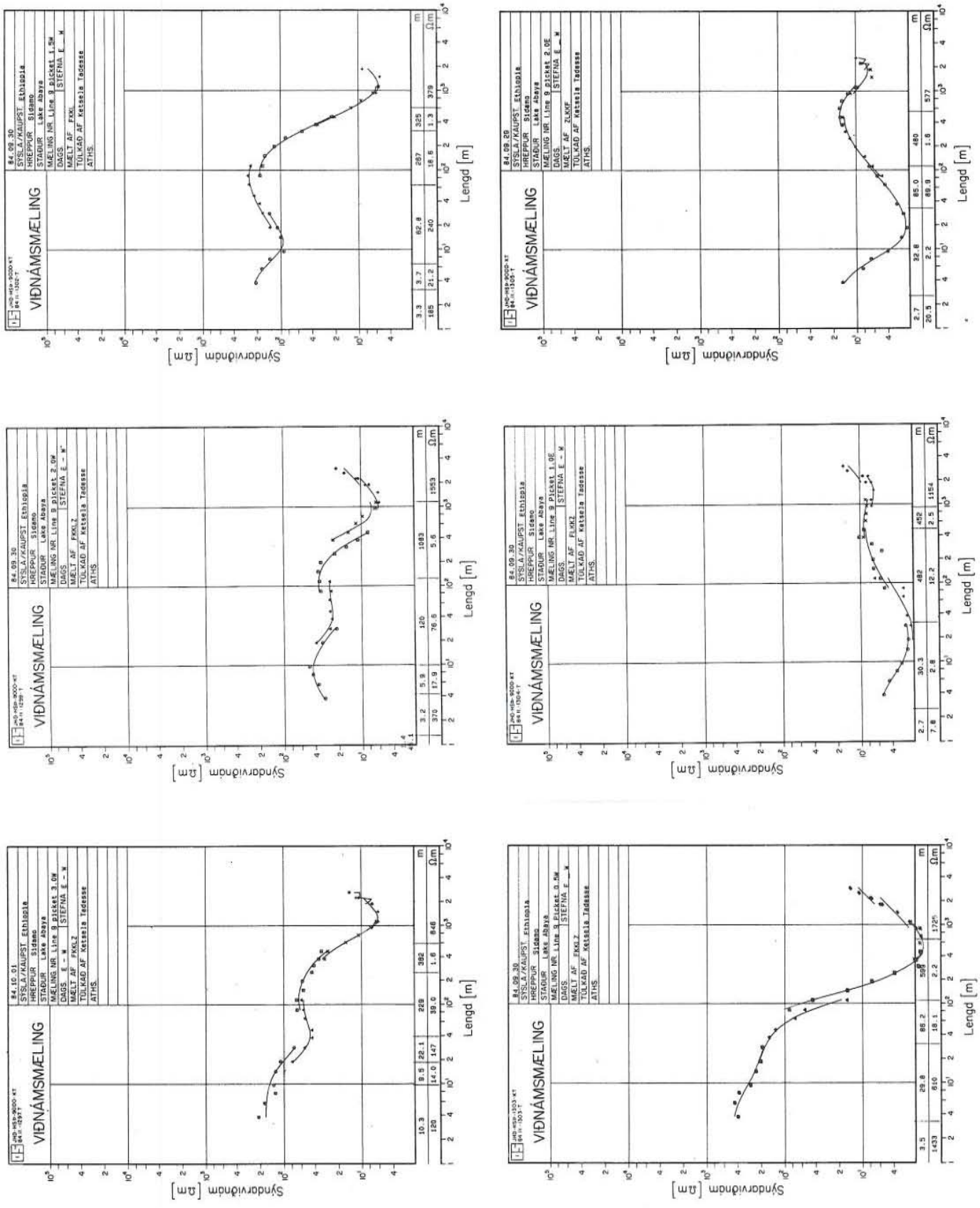

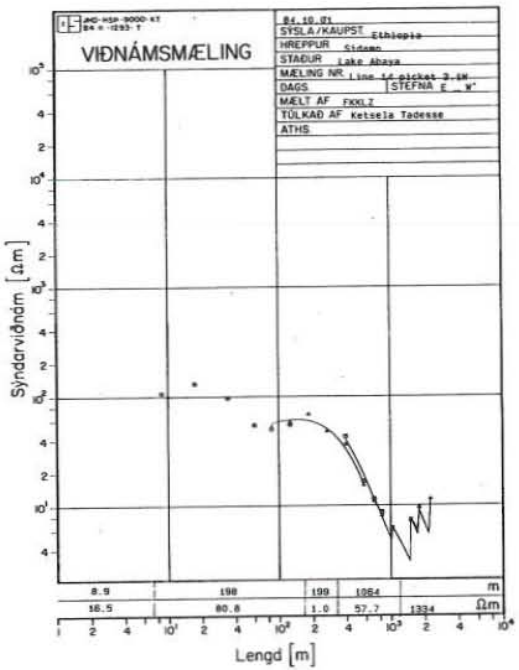
VIÐNÁMSMÆLING
84.10.01
SÝSLA/KAUPST. Ethiopia
HREPPUR Sidamo
STAÐUR Lake Abaya
MÆLING NR. Line 14 picket 3.1W
DAGS. STEFNA E _ W
MÆLT AF FKKLZ
TÚLKAÐ AF Ketsela Tadesse
ATHS.
Sýndarviðnám [Ωm]
Lengd [m]

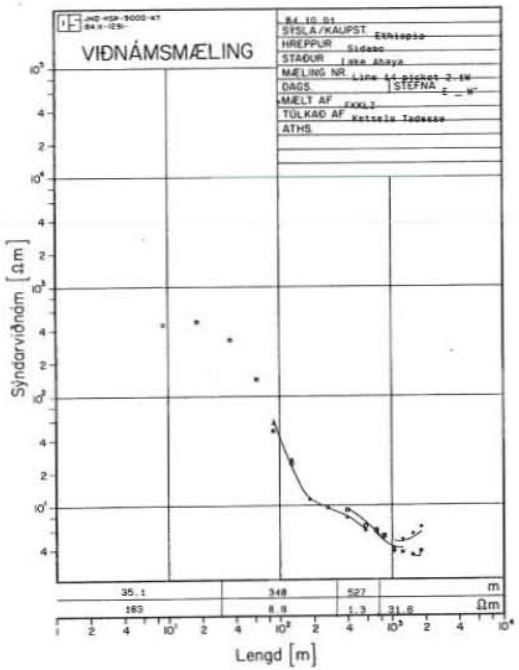
VIÐNÁMSMÆLING
84.10.01
SÝSLA/KAUPST. Ethiopia
HREPPUR Sidamo
STAÐUR Lake Abaya
MÆLING NR. Line 14 picket 2.1W
DAGS. STEFNA E _ W
MÆLT AF FKKLZ
TÚLKAÐ AF Ketsela Tadesse
ATHS.
Sýndarviðnám [Ωm]
Lengd [m]

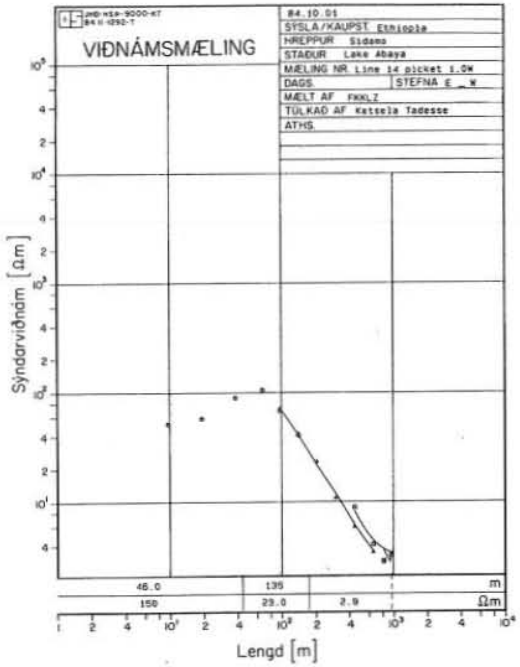
VIÐNÁMSMÆLING
84.10.01
SÝSLA/KAUPST. Ethiopia
HREPPUR Sidamo
STAÐUR Lake Abaya
MÆLING NR. Line 14 picket 1.0W
DAGS. STEFNA E _ W
MÆLT AF FKKLZ
TÚLKAÐ AF Ketsela Tadesse
ATHS.
Sýndarviðnám [Ωm]
Lengd [m]

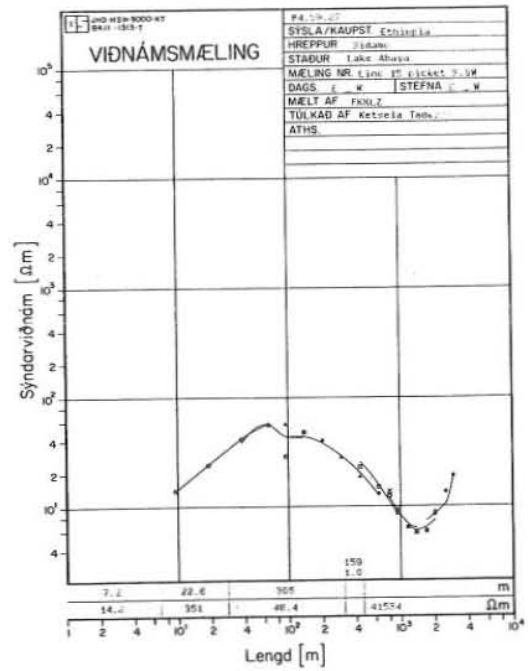
VIÐNÁMSMÆLING
84.09.27
SÝSLA/KAUPST. Ethiopia
HREPPUR Sidamo
STAÐUR Lake Abaya
MÆLING NR. Line 15 picket 3.1W
DAGS. STEFNA E _ W
MÆLT AF FKKLZ
TÚLKAÐ AF Ketsela Tadesse
ATHS.
Sýndarviðnám [Ωm]
Lengd [m]

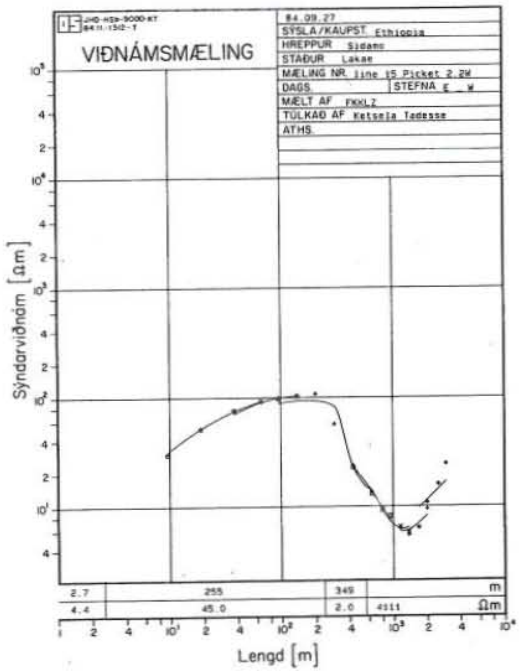
VIÐNÁMSMÆLING
84.09.27
SÝSLA/KAUPST. Ethiopia
HREPPUR Sidamo
STAÐUR Lakae
MÆLING NR. Line 15 Picket 2.2W
DAGS. STEFNA E W
MÆLT AF FKKLZ
TÚLKAÐ AF Ketsela Tadesse
ATHS.
Sýndarviðnám [Ωm]
Lengd [m]

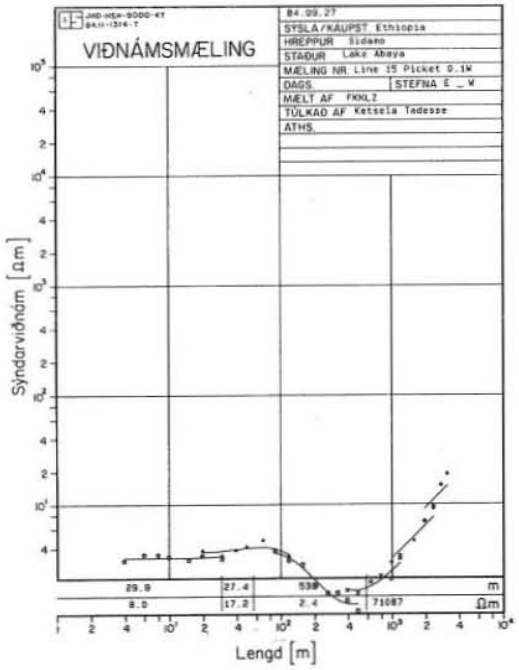
VIÐNÁMSMÆLING
84.09.27
SÝSLA/KAUPST. Ethiopia
HREPPUR Sidamo
STAÐUR Lake Abaya
MÆLING NR. Line 15 Picket 0.1W
DAGS. STEFNA E _ W
MÆLT AF FKKLZ
TÚLKAÐ AF Ketsela Tadesse
ATHS.
Sýndarviðnám [Ωm]
Lengd [m]

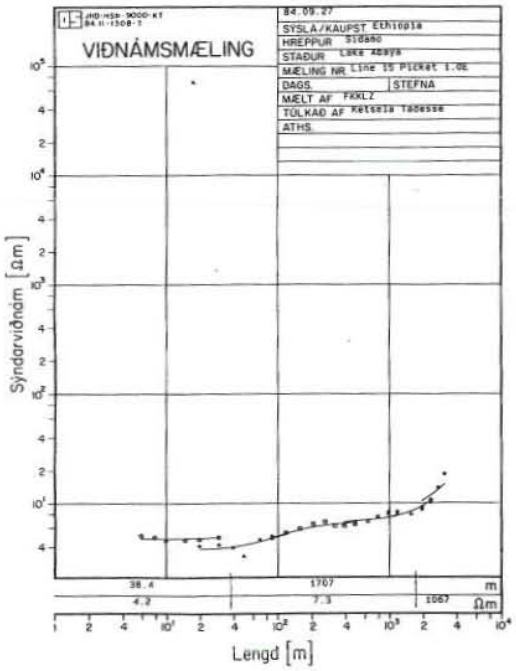
VIÐNÁMSMÆLING
84.09.27
SÝSLA/KAUPST Ethiopia
HREPPUR Sidamo
STAÐUR Lake Abaya
MÆLING NR. Line 15 Picket 1.0E
DAGS. STEFNA
MÆLT AF FKKLZ
TÚLKAÐ AF Ketsela Tadesse
ATHS.
Sýndarviðnám [Ωm]
Lengd [m]

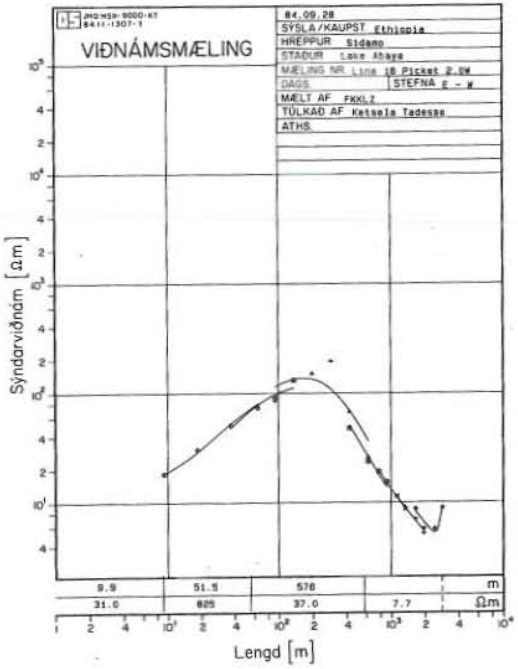
VIÐNÁMSMÆLING
84.09.28
SÝSLA/KAUPST Ethiopia
HREPPUR Sidamo
STAÐUR Lake Abaya
MÆLING NR. Line 16 Picket 2.0W
DAGS. STEFNA E - W
MÆLT AF FKKLZ
TÚLKAÐ AF Ketsela Tadesse
ATHS.
Sýndarviðnám [Ωm]
Lengd [m]

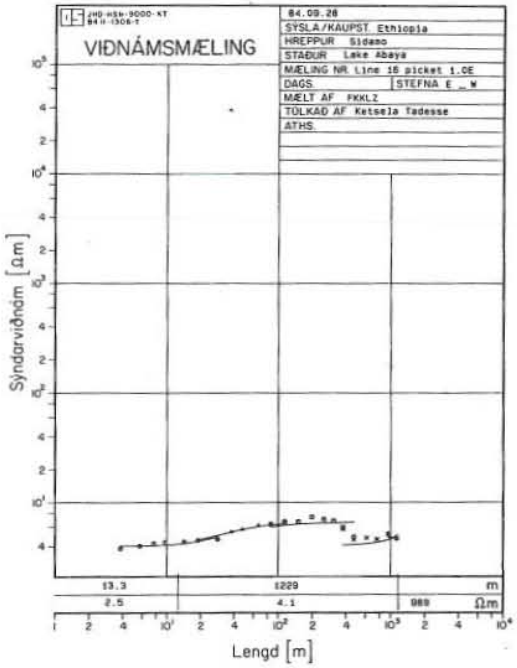
VIÐNÁMSMÆLING
84.09.28
SÝSLA/KAUPST Ethiopia
HREPPUR Sidamo
STAÐUR Lake Abaya
MÆLING NR. Line 16 picket 1.0E
DAGS. STEFNA E _ W
MÆLT AF FKKLZ
TÚLKAÐ AF Ketsela Tadesse
ATHS.
Sýndarviðnám [Ωm]
Lengd [m]

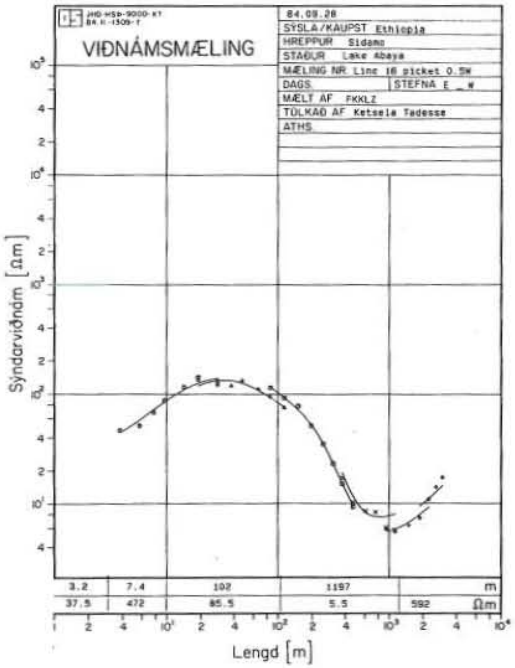
VIÐNÁMSMÆLING
84.09.28
SÝSLA/KAUPST Ethiopia
HREPPUR Sidamo
STAÐUR Lake Abaya
MÆLING NR. Line 16 picket 0.5W
DAGS. STEFNA E _ W
MÆLT AF FKKLZ
TÚLKAÐ AF Ketsela Tadesse
ATHS.
Sýndarviðnám [Ωm]
Lengd [m]

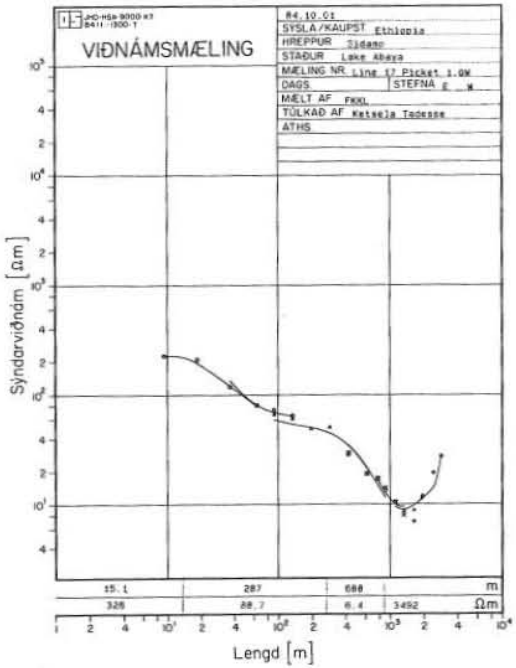
VIÐNÁMSMÆLING
84.10.01
SÝSLA/KAUPST Ethiopia
HREPPUR Sidamo
STAÐUR Lake Abaya
MÆLING NR. Line 17 Picket 1.0W
DAGS. STEFNA E _ W
MÆLT AF FKKL
TÚLKAÐ AF Ketsela Tadesse
ATHS.
Sýndarviðnám [Ωm]
Lengd [m]

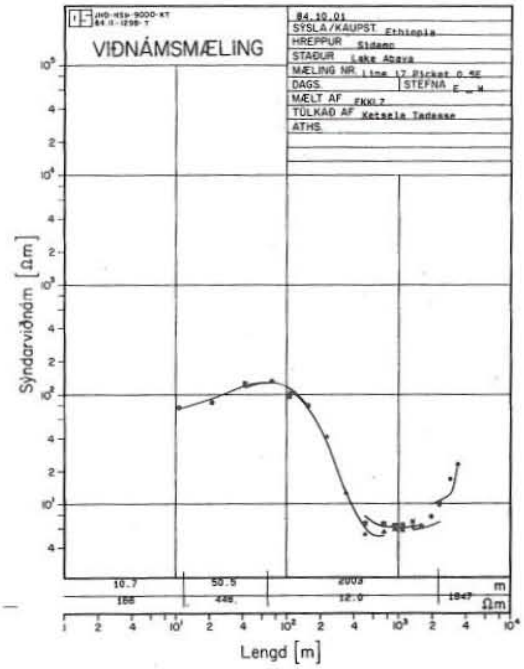
VIÐNÁMSMÆLING
84.10.01
SÝSLA/KAUPST Ethiopia
HREPPUR Sidamo
STAÐUR Lake Abaya
MÆLING NR. Line 17 Picket 0.5E
DAGS. STEFNA E _ W
MÆLT AF FKKLZ
TÚLKAÐ AF Ketsela Tadesse
ATHS.
Sýndarviðnám [Ωm]
Lengd [m]

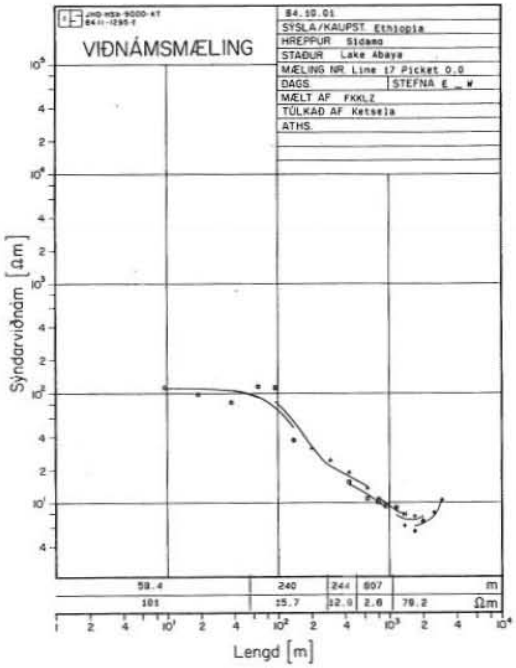
VIÐNÁMSMÆLING
84.10.01
SÝSLA/KAUPST. Ethiopia
HREPPUR Sidamo
STAÐUR Lake Abaya
MÆLING NR. Line 17 Picket 0.0
DAGS. STEFNA E _ W
MÆLT AF FKKLZ
TÚLKAÐ AF Ketsela
ATHS.
Sýndarviðnám [Ωm]
Lengd [m]

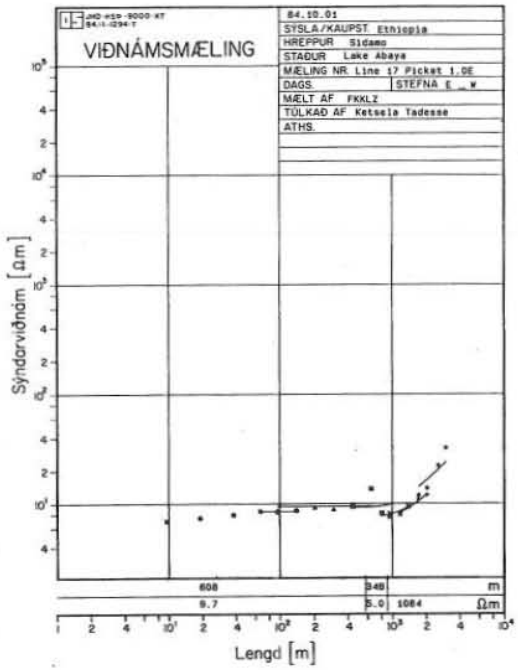
VIÐNÁMSMÆLING
84.10.01
SÝSLA/KAUPST. Ethiopia
HREPPUR Sidamo
STAÐUR Lake Abaya
MÆLING NR. Line 17 Picket 1.0E
DAGS. STEFNA E _ W
MÆLT AF FKKLZ
TÚLKAÐ AF Ketsela Tadesse
ATHS.
Sýndarviðnám [Ωm]
Lengd [m]

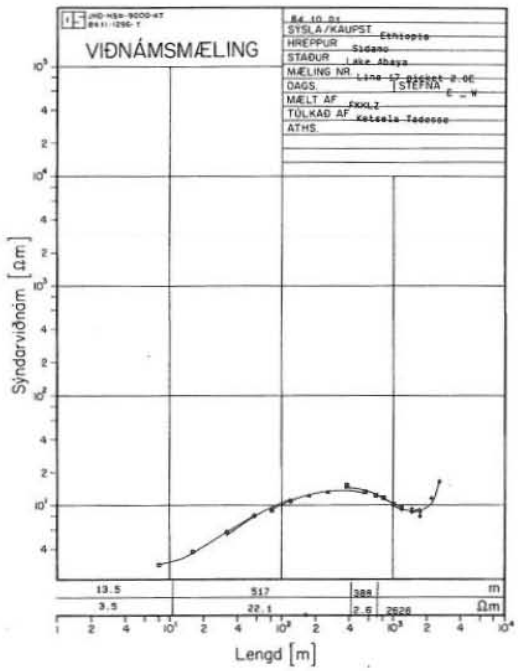
VIÐNÁMSMÆLING
84.10.01
SÝSLA/KAUPST. Ethiopia
HREPPUR Sidamo
STAÐUR Lake Abaya
MÆLING NR. Line 17 picket 2.0E
DAGS. STEFNA E _ W
MÆLT AF FKKLZ
TÚLKAÐ AF Ketsela Tadesse
ATHS.
Sýndarviðnám [Ωm]
Lengd [m]

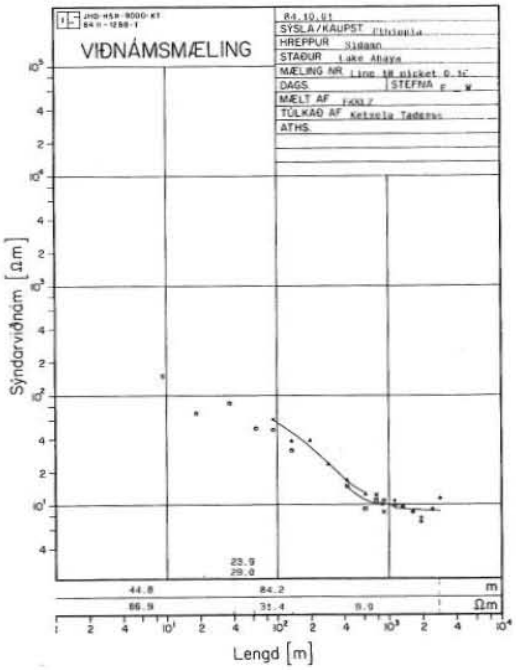
VIÐNÁMSMÆLING
84.10.01
SÝSLA/KAUPST. Ethiopia
HREPPUR Sidamo
STAÐUR Lake Abaya
MÆLING NR. Line 18 picket 0.1E
DAGS. STEFNA E _ W
MÆLT AF FKKLZ
TÚLKAÐ AF Ketsela Tadesse
ATHS.
Sýndarviðnám [Ωm]
Lengd [m]

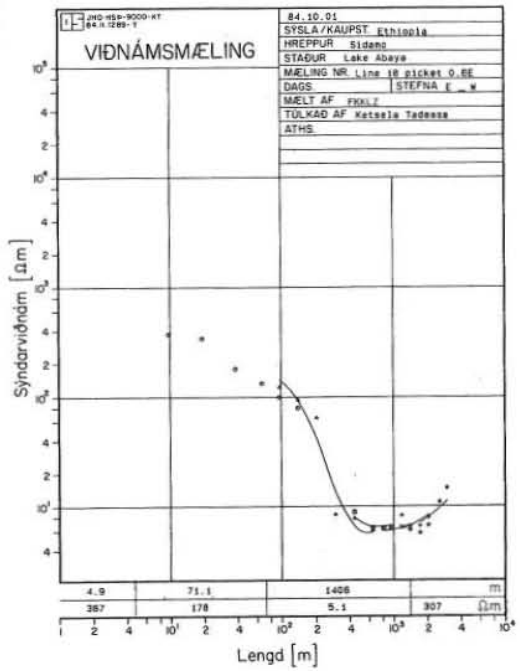
VIÐNÁMSMÆLING
84.10.01
SÝSLA/KAUPST. Ethiopia
HREPPUR Sidamo
STAÐUR Lake Abaya
MÆLING NR. Line 18 picket 0.8E
DAGS. STEFNA E _ W
MÆLT AF FKKLZ
TÚLKAÐ AF Ketsela Tadesse
ATHS.
Sýndarviðnám [Ωm]
Lengd [m]

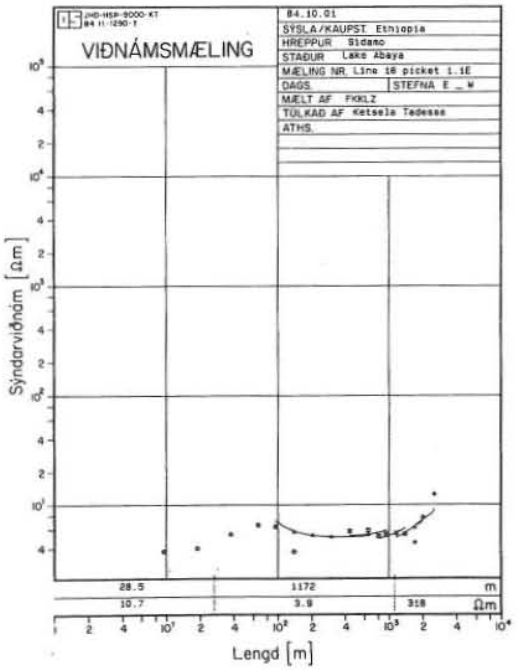
VIÐNÁMSMÆLING
84.10.01
SÝSLA/KAUPST. Ethiopia
HREPPUR Sidamo
STAÐUR Lake Abaya
MÆLING NR. Line 18 picket 1.1E
DAGS. STEFNA E _ W
MÆLT AF FKKLZ
TÚLKAÐ AF Ketsela Tadesse
ATHS.
Sýndarviðnám [Ωm]
Lengd [m]

APPENDIX II

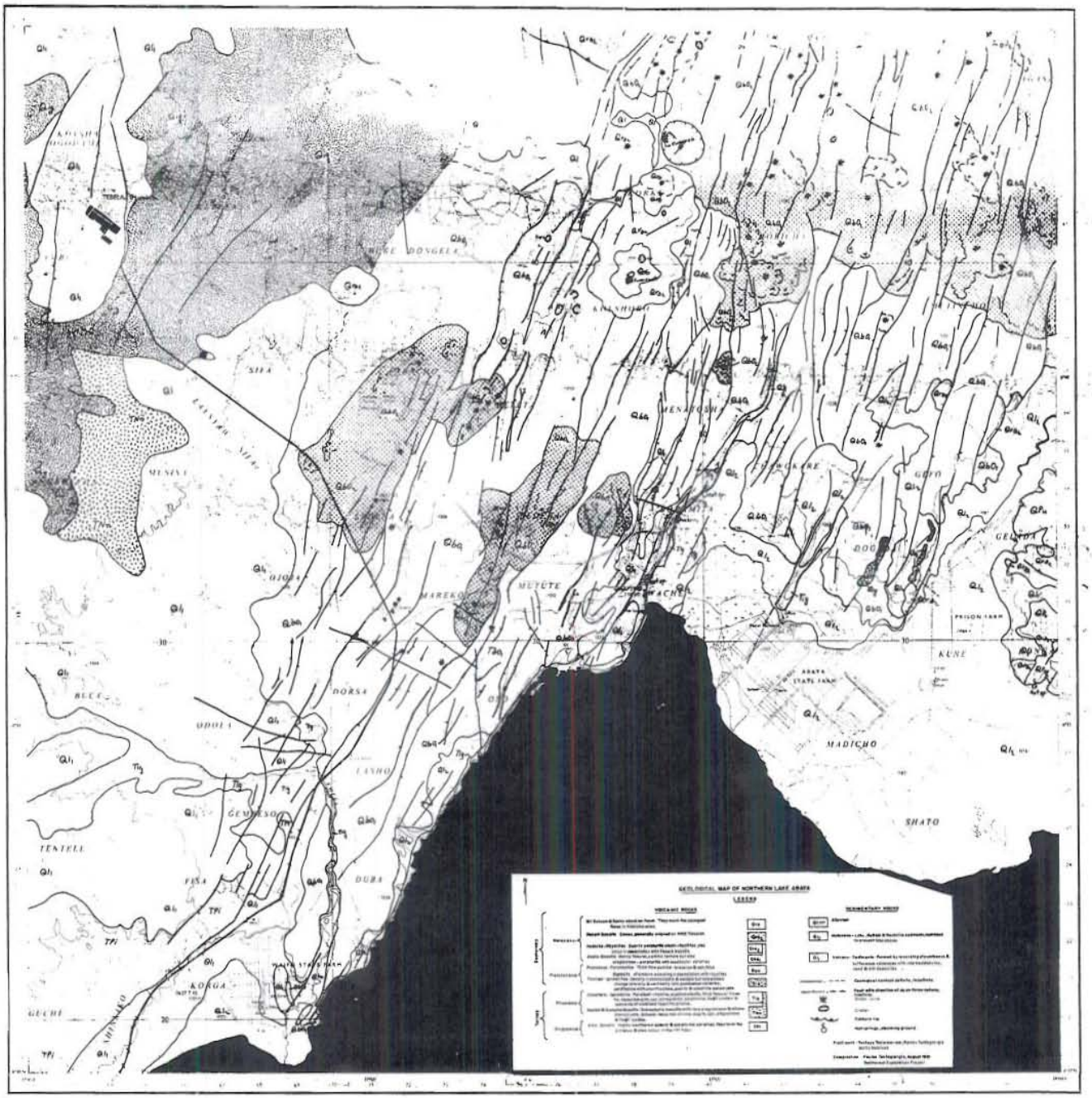

Geological map of northern Lake Abaya.